

INVESTIGATING THE EFFECTS OF MECHANICAL DAMAGE ON THE ELECTRICAL RESPONSE OF LI-ION POUCH CELLS

A Thesis
Submitted to
the Temple University Graduate Board

In Partial Fulfillment
of the Requirements for the Degree
MASTER OF SCIENCE IN
MECHANICAL ENGINEERING

by
Andrew W. Stacy
December 2019

Thesis Approvals:

Damoon Soudbakhsh, Thesis Advisor, Department of Mechanical Engineering

Daniel Jacobs, Department of Mechanical Engineering

Elham Sahraei, Department of Mechanical Engineering

Parsaoran Hutapea, Department of Mechanical Engineering

ABSTRACT

Li-ion batteries (LIB) are used in many applications because of their high-power/energy density, long life cycling, and low self-discharge rate. The use of LIB continues to grow every day, and the necessity for proper safety standards grows as well. A key aspect for safe utilization of LIB is determining their safety and remaining useful life (RUL). Battery characteristics degrade over time under normal and extreme operating conditions and modeling the electrochemical processes can improve RUL estimations. Extreme operating conditions such as abnormal temperatures and charge/discharge rates are believed to exacerbate the rate of degradation. Li-ion batteries are also susceptible to mechanical damage, which may lead to an electrical short. In severe cases, mechanical damage causes a thermal run away, and possibly explosions or fires. In the event of a car accident, battery packs can be damaged without an electrical short or immediate thermal run away. Currently, there is no reliable battery characterization method to determine safety of the battery packs for future use after sustaining mechanical damage. The obvious gap in LIB technology and safety can be bridged by predictive dynamic models for individual cells. In this study, we construct an equivalent circuit model (ECM) based on electrochemical processes that utilizes a combination of resistors, inductor, constant phase elements, and a Warburg impedance element. Three separate mechanical deformations are introduced to Li-ion pouch cells and subsequently modeled. These experiments show the possibility of detecting mechanical damage in Li-ion pouch cells prior to an electrical short. The results from this study can have a major impact in advancing on-invasive fault detection capabilities for battery management systems used in many commercial LIB applications.

ACKNOWLEDGEMENTS

I would first like to thank Dr. Damoon Soudbakhsh for giving me the opportunity to show my value to the engineering community. He has guided me with expertise throughout my research by supplying the necessary literature and in-depth explanations. I must also express gratitude to Dr. Mehdi Gilaki, his expertise on Li-ion battery safety has been critical to the design and implementation of reliable experiments. With his guidance, we were able to draw valuable conclusions on the effects mechanical damage has on the electrical response of Li-ion pouch cells. Lastly, I would like to thank the thesis committee and Temple University's Engineering staff for their devotion to student success.

TABLE OF CONTENTS

ABSTRACT.....	i
ACKNOWLEDGEMENTS.....	ii
LIST OF FIGURES	iv
LIST OF TABLES.....	vi
NOMENCLATURE	vii
CHAPTER 1- INTRODUCTION.....	1
1.1 Background.....	1
1.2 Problem Statement.....	4
1.3 Scope of Research.....	5
1.4 Instrumentation	6
1.5 Li-ion Pouch Cell Holder.....	6
1.6 EIS Measurement and ECM Validations.....	9
1.7 Summary.....	10
CHAPTER 2 – ELECTROCHEMICAL BASED EQUIVALENT CIRCUIT MODEL.....	11
2.1 Proposed Electrochemical Based ECM	11
2.2 Fitting Techniques	15
2.3 Fitting Method for Proposed ECM	18
CHAPTER 3 – CONTROLLED MECHANICAL DAMAGE WITH LOW C-RATE CYCLING	21
3.1 Method and Set-up.....	21
3.2 Results.....	25
3.3 Summary	28
CHAPTER 4 – STEP INDENTATION WITH HEMI-SPHERICAL PUNCH.....	29
4.1 Method and set-up.....	29
4.2 Results.....	30
4.3 Summary	37
CHAPTER 5 – STEP MECHANICAL THREE POINT BENDING.....	38
5.1 Method and set-up.....	38
5.2 Results.....	39
5.3 Summary	45
DISCUSSION AND CONCLUSION.....	46
REFERENCES	49

LIST OF FIGURES

Figure 1: Pouch cell holder	7
Figure 2: Cross sectional view of pouch cell holder.....	8
Figure 3: Distributed ECM for Li-Ion pouch cell.....	12
Figure 4: Li-ion pouch cell connection to Gamry 30k Booster for EIS measurements...	23
Figure 5: Punch test set-up and final 2.8-mm indentation	24
Figure 6: Experimental data fitted to the proposed ECM and K-K transforms (a) Nyquist (b) Bode	25
Figure 7: Trend changes of ECM parameter values throughout charge/discharge EIS measurements: (a) inductance, (b) ohmic resistance, (c) solid electrolyte interface resistance, (d) Q_{CPE} of the SEI layer, (e) conditioning number of the SEI layer and (f) charge transfer resistance.....	27
Figure 8: Trend changes of ECM parameter values throughout charge/discharge EIS measurements: (a) double layer Q_{CPE} , (b) double layer conditioning number, (c) bounded Warburg element and (d) OCV	28
Figure 9: Step indentation set-up and connection to Gamry 30k booster for EIS measurements.....	30
Figure 10: Trend changes of ECM parameter values throughout step indentation and control cell EIS measurements: (a) inductance, (b) ohmic resistance, (c) solid electrolyte interface resistance and (d) Q_{CPE} of the SEI layer	32
Figure 11: Trend changes of ECM parameter values throughout step indentation and control cell EIS measurements: (a) conditioning number of the SEI layer, (b) charge transfer resistance, (c) double layer Q_{CPE} , (d) double layer conditioning number, (e) bounded Warburg element and (f) OCV.....	33
Figure 12: Force vs displacement during step indentation	35
Figure 13: Trend changes of ECM parameter values vs depth throughout step indentation EIS measurements: (a) inductance, (b) ohmic resistance, (c) solid electrolyte interface resistance and (d) Q_{CPE} of the SEI layer	35
Figure 14: Trend changes of ECM parameter values vs depth throughout step indentation EIS measurements: (a) conditioning number of the SEI layer, (b) charge transfer resistance, (c) double layer Q_{CPE} , (d) double layer conditioning number and (e) bounded Warburg element and (f) OCV.....	36
Figure 15: Three-point bending set-up and connection to Gamry 30k booster for EIS measurements.....	39

- Figure 16: Trend changes of ECM parameter values throughout three point bending and control cell EIS measurements: (a) inductance, (b) ohmic resistance, (c) solid electrolyte interface resistance and (d) Q_{CPE} of the SEI layer 40
- Figure 17: Trend changes of ECM parameter values throughout three point bending and control cell EIS measurements: (a) conditioning number of the SEI layer, (b) charge transfer resistance, (c) double layer Q_{CPE} , (d) double layer conditioning number, (e) bounded Warburg element and (f) OCV 41
- Figure 18: Force applied vs displacement of cell 3 during three-point bending 43
- Figure 19: Trend changes of ECM parameter values vs depth throughout three point bending EIS measurements: (a) inductance, (b) ohmic resistance, (c) solid electrolyte interface resistance and (d) Q_{CPE} of the SEI layer 43
- Figure 20: Trend changes of ECM parameter values vs depth throughout three point bending EIS measurements: (a) conditioning number of the SEI layer, (b) charge transfer resistance, (c) double layer Q_{CPE} , (d) double layer conditioning number (e) bounded Warburg element and (f) OCV 44

LIST OF TABLES

Table 1: Shorted lead test for Li-Ion Pouch cell.....	8
Table 2: Parameter values used to estimate value for diffusion coefficient of Li-ion pouch cell (Eq. 17).....	19
Table 3: Initial Fitting Parameters for Simplex Method.....	20

NOMENCLATURE

Parameter	Description	Unit
$R_{t,Li}$	Charge transfer resistance	$Ohm \cdot cm^2$
K_{Li}	Reaction rate constant	$\frac{m^{5/2}}{s\sqrt{mol}}$
b_{Li}	Kinetic parameter	V^-
α_{Li}	Symmetry factor	—
n	Number of electrons transferred per mol of reaction species	—
F	Faraday's constant	$\frac{Coulombs}{equivalent}$
R	Universal gas constant	$\frac{J}{mol K}$
T	Temperature	$^{\circ}K$
\bar{V}	Steady state voltage	V
σ	Warburg diffusion coefficient	$\frac{ohm}{\sqrt{s}}$

Parameter	Description	Unit
D_{Li}	Diffusion coefficient for Li ⁺ ion	$\frac{m^2}{mol}$
c	Li ⁺ ion concentration	$\frac{mol}{m^3}$
i_p	Peak current	A
A	Area of electrodes	cm^2
ω	Frequency	$\frac{rad}{s}$
i_0	Exchange Current Density	$\frac{A}{cm^2}$

CHAPTER 1- INTRODUCTION

In this chapter an introduction to LIB applications and current research in this field will be presented. Following a background discussion, reasons for studying the electrical response of LIB subjected to mechanical damage is conveyed. The final section in this chapter will introduce the reader to fundamental concepts used to study the Li-ion pouch cells throughout this document.

1.1 Background

Li-Ion Batteries are the preferred power source for many applications including cell phones, electric vehicles, hybrid electric vehicles, electric powertrain, grid storage, and many more. The possibilities for advantageous use of LIB is vast because they have high power/energy density, long cycling life, and low self-discharge rate [1], [2]. These batteries do not come without hazard. Under abuse conditions an uncontrollable release of large amounts of energy can occur. This creates safety issues that need to be addressed [3], [4]. Accidental abuse and mechanical loading on LIB are inevitable in applications such as electric vehicles, and batteries that are damaged in accidents have the potential for thermal runaway [5]. Research on pouch and cylindrical cells have quantified the mechanical damage required to cause an internal short, called critical depth of deformation [6]–[18]. This occurs when principle strain components of the battery cell exceed their failure limits [19], [20].

Although a critical depth of deformation can be found for Li-Ion batteries, it does not characterize what occurs prior to battery failure. Research has shown that micro fractures in electrode coating and thinning of the battery separators form long before failure. The

previously described damage to LIB where mechanical deformations do not lead to immediate failure is missing from current literature. Pre-failure deformation of a LIB may affect electrochemical performance of cells. This study investigates if by measuring the electrical response of a cell after a vehicle sustains abusive loading or impact, mechanical damage to cells can be detected. The mission is to determine whether a battery is safe or potentially harmful after sustaining mechanical damage. Along with potential safety hazards being detected the cells RUL can be estimated.

This study will lay the foundation for the estimation of LIB State of Health (SoH) using ECM parameters. A batteries State of Health can be defined as the degradation of ECM parameters after electrical cycling and ageing in different environments. In some studies [21], researchers use the internal resistance and capacity fade to estimate the batteries SoH. Many studies hope to use nonlinear elements for dynamical modeling of battery parameters. Dynamic methods for SoH estimation include pulse tests followed by DC voltage measurements and Electrochemical Impedance Spectroscopy (EIS) [22],[23]. Electrochemical Impedance Spectroscopy is the chosen method for this study because it provides more data with a wider frequency range. Influences from temperature and state of charge (SoC) on EIS measurement must be noted. It has been shown that colder temperatures result in wider EIS plots [22], [24]. A cells SoC will alter EIS data in various ways. The effects of SoC on ECM parameters can be seen in [25]. Another influence on EIS measurements is the relaxation time after electrical loading [1]. Although this influence is known there is little study on optimal relaxation time. There have been many studies on intact batteries, such studies characterize and model battery degradation over time.

However, there has been little research done to characterize the effects of mechanical damage on trend changes in ECM parameters.

Equivalent circuit models fall under three main categories for modeling the dynamic response of LIB. They can be separated into simple, phenomenological, and electrochemical process-based methods [26]. Simple ECM is the most popular modeling procedure, because the approximation of battery characteristics is sufficient for low power batteries. Phenomenological ECM is an extension from a simple model where pulses are used to determine parameter values and stored in a look up table to characterize the batteries response. Both models use external influences such as SOC and temperature to more accurately model the electrical response. These two methods for modeling LIB have two main drawbacks. One is that the physicality of the system is lost. This is because each does not account for the electrochemical processes occurring in the battery, therefore they lose accuracy when modeling high powered batteries. The second drawback is the lack of extrapolation for these models because the ECM parameters become mere fitting parameters and cannot be extended into wider frequency ranges.

These two models have clear drawbacks for modeling high powered batteries and accurately modeling unknown frequencies. Electrochemical process-based methods can be used to connect the ECM parameters to physicality of the battery. By connecting the physics of the battery to the ECM, we can produce a model that will accurately determine parameters for various frequency ranges. This study will use electrochemical processes and known characteristics of a Li-ion pouch cell to construct a model and fitting procedure to accurately and consistently fit ECM parameters.

1.2 Problem Statement

There is no current method for non-invasive detection of mechanical damage in Li-ion pouch cells. Pouch cells have been used extensively in many electric and hybrid vehicles such as the Chevy Volt and Nissan Leaf. In the case of an accidents or damages to the battery pack, there currently is no effective method to detect damaged cells and as a result in many situations the whole battery pack needs to be replaced and the vehicle should be abandoned and towed [25]. Typically, battery diagnostic systems detect electrical failures such as short circuits and loose connections; and research on detecting mechanical damage to Li-ion batteries has been very limited [27]. We propose quantifying damages to the pouch cells using EIS, which provides a response of the battery to a wide range of excitation frequencies. Using EIS data combined with cycling data, we can develop accurate models of the cells and use data analytics tools to detect mechanical damages and the remaining useful life of the cells.

1.3 Scope of Research

The Li-ion cells used in this study are from the battery pack of a Chevy Volt Gen 2 hybrid electric vehicle. The cells starting capacitance is 26.3 A/hr. This capacitance is calculated from charge and discharge data. Maccor software integrates the current versus time curve, therefore finding the area under the curve and the equivalent capacitance. The cells 100% state of charge (SOC) voltage is 4.1 V, and 0% SOC voltage is 3.0 V. It is produced using graphite-based chemistry with a liquid carbonate electrolyte [28]. The cell in this study has the dimensions of 231.78 mm x 163.51 mm x 7.66 mm, and the dimensions of the electrode tabs are as follow; 6.145mm long x 44.80 mm wide x 0.20 mm thick and separated by 36.10 mm.

In this study, we will perform three separate experiments subjecting the Li-ion pouch cell previously described to various mechanical loading and experimental methods. For each experiment the proposed electrochemical-based ECM is used to model experimental data. The first experiments discussed in this study subjects a cell to a hemi-spherical punch and cycling at low C-rate to characterize the difference between intact and indented cells. Next, we will discuss subjecting the previously indented cell to the same form of mechanical damage until an electrical short occurs. Electrochemical impedance spectroscopy measurements were collected intermittently between indentation depths so that any changes in ECM parameters could be detected. The last experiment in this study, exposed a cell to an ideal three-point bending scenario, where again EIS measurements were taken intermittently. In this study, the cell was not damaged until failure but until a specific depth discussed in chapter 5.

1.4 Instrumentation

Electrochemical Impedance Spectroscopy was performed using Gamry's Reference 3000 in conjunction with the Reference 30k Booster. The instruments have the capability to accurately measure values below 100 microohms on a range of 300 kHz to 10 μ Hz. The 30k Booster has a ± 30 A current output with an accuracy of $\pm 0.2\%$. Cycling was performed using the Maccor 4200, it has the capability of cycling on eight channels. Each channel has a current range of ± 15 A with accuracy of $\pm 0.025\%$ full scale (FS), and a voltage range of 0 to 20 V ± 4 mV with an accuracy of $\pm 0.02\%$ FS. The Maccor 4200 has a 16-bit resolution and minimum step time of 10 ms. The cells were placed in holders designed specifically for these pouch cells.

1.5 Li-ion Pouch Cell Holder

When performing EIS on low-impedance Li-ion cells a major problem is that measurements are more susceptible to external influences. These influences can distort data, so it is important to have a fixture for the Li-ion cell that creates a repeatable connection [29]. To overcome this challenging characteristic of the studied cells, a pouch cell holder was designed and manufactured.

When designing the pouch cell holder, four main design characteristics were considered: (i) a four-electrode connection, (ii) flexibility to connect to both data collection instruments, (iii) portability, and (iv) low impedance. It is important for the cell holder to have a four-electrode connection because it was the chosen connection method for all experiments in this study. The pouch cell holder designed for this study allows for two connections on each electrode, one sense and one current carrying lead. It is designed to directly connect

to the Gamry EIS instruments, reducing any unnecessary wiring and therefore minimizing external influences on data. To allow for the pouch cell to be connected to the Gamry 30k booster and the Maccor independently, external fixtures were designed for connection to the Maccor via alligator clips. The holder was also designed to permit movement between location without disconnecting the cell from the holder. This design requirement was achieved by using a rubber strap to secure the cell pouch flatly on the holder, while a bolt directly between the electrodes secure them into position on the copper plate, see Figure 1 and Figure 2. One final key characteristic of the pouch cell holder is the low measurable impedance. To ensure the holder has very low impedance, it was designed using super conductive copper with purity of 99.99%.



Figure 1: Pouch cell holder

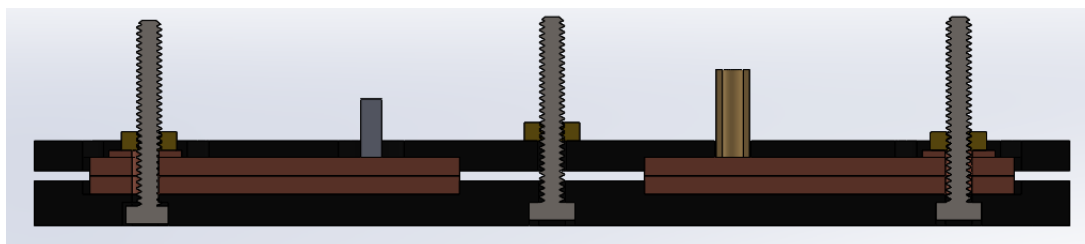


Figure 2: Cross sectional view of pouch cell holder

The holder was developed using a pouch cell to test accuracy, reproducibility, and reliability of acquired EIS data when connected to the holder. The final design was manufactured in house for each cell. Prior to data collection, a shorted lead test was performed on each holder to test for consistency in manufacturing. Shorted lead tests capture the resistance and inductance produced by wires, instruments, and fixtures [29]. It is performed by taking EIS measurements of the set-up with a short between the positive and negative terminals of the cell holder. In this study, the shorted lead used was a small copper plate, it was placed in position and fastened down to replicate the pouch cells connection. A frequency range of 2 kHz to 10 mHz was used in galvanostatic EIS measurements, with an excitation current of 10 A. The holders shorted lead spectrums are all within $50 \mu\Omega$, (see Table 1).

Table 1: Shorted lead test for Li-Ion Pouch cell

<i>Holder Number</i>	Inductance (Henry)	Resistance (Ohms)
1	41.22e-9	104.0e-6
2	40.70e-9	134.0e-6
3	42.25e-9	126.0e-6
4	42.82e-9	146.0e-6

1.6 EIS Measurement and ECM Validations

Kramers-Kronig (K-K) transforms are used to validate the quality of every EIS measurement taken in this study. K-K transforms conclude the following four conditions of a system are satisfied; causality, stability, linearity and fitness of response [29]. Causality states that any response to the system is a direct response to applied perturbations. Stability is the condition that the system doesn't change over time and that it returns to the original state following perturbations. Linearity verifies that the system follows ohms law, and that the magnitude of impedance is independent of the perturbations to the system. Linearity in batteries is a good approximation if the applied excitation voltage is below 20 mV. Where in this study a 10 mV excitation voltage was used. If all these conditions are met, then the imaginary and real components of impedance are interdependent. K-K transforms can be related to the frequency domain as follows in (1), (2) [23], [30];

$$\hat{Z}_R(\omega) = R_0 + \frac{2}{\pi} \int_0^{\infty} \frac{xZ_I(x) - \omega Z_I(\omega)}{x^2 - \omega^2} dx \quad (1)$$

$$Z_I(\omega) = \frac{2\omega}{\pi} \int_0^{\infty} \frac{Z_R(x) - Z_R(\omega)}{x^2 - \omega^2} dx \quad (2)$$

To quantify the goodness of fit for the ECM, a sum of weighted errors χ^2 is performed. The sum of weighted errors χ^2 quantifies the difference between collected data and the proposed model data for impedance measurements of the same frequency. For this study, we required the weighted error in (3) to be less than 10^{-4} , where Z_{RE} and Z_{IE} are expected real and imaginary parts of impedance from fitted model.

$$\chi^2 = \sum_{i=1}^n \left(\frac{(Z_{i,R} - Z_{i,RE})^2}{Z_{i,RE}^2} + \frac{(Z_{i,I} - Z_{i,IE})^2}{Z_{i,IE}^2} \right) \quad (3)$$

Other characteristics taken into account when evaluating the models validity are the physicality of each component, component error, and random residuals [29]. Physicality of each component refers to each element in the ECM to have a real-world electrochemical phenomenon associated with it. Having the majority of components with error values less than the modeled element value is important to conclude the model is correctly modeling the electrochemical phenomena. Finally, random residuals show that the model is not systematically producing errors as opposed to random errors being produced.

1.7 Summary

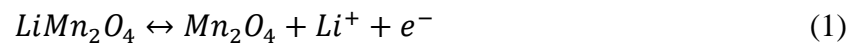
In this chapter we discussed the necessity for non-invasive fault detection in LIB that have been subjected to mechanical damage. We included a description of the cells being studied and the holder designed to connect Li-ion pouch cells to data collection instrumentation. We showed that the cell holders used in this study are of the same quality and have little effects on EIS measurements. This chapter also entails methods used throughout to verify data quality of EIS measurement and goodness of fit to the proposed electrochemical process-based ECM.

CHAPTER 2 – ELECTROCHEMICAL BASED EQUIVALENT CIRCUIT MODEL

In this chapter, we present the electrochemical process-based ECM used to fit EIS measurements in this study. Characteristics of the electrochemical processes will be discussed, along with techniques to estimate values. Following this discussion, the fitting procedure used for study will be defined.

2.1 Proposed Electrochemical Based ECM

The critical chemical reaction in a Li-ion battery is a redox reaction involving the transfer of electrons between chemical species. Li^+ ions are extracted from the cathode and absorbed by the anode during charging, while electrons pass through the circuit powering a given load. The transfer process depends on both the cathode and anode, yet the limiting factor for LIB comes from the cathode side. For this study the chemical reaction is as follows (1) [31].



The equivalent circuit model for this study can be seen in Figure 3, it consists of passive elements to replicate a complex non-linear electrical circuit. This ECM is proposed in [25], [32]. Each element in the ECM can be attributed to one of five electrochemical phenomena occurring in the cell: loss of conductivity, solid electrolyte interface formation, charge transfer resistance, double layer capacitance and finite diffusion.

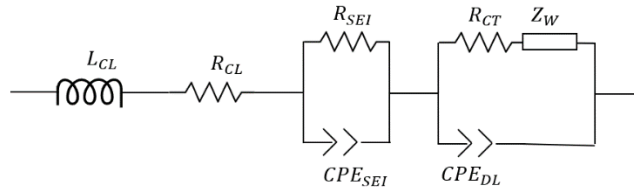


Figure 3: Distributed ECM for Li-Ion pouch cell

The inductor L_{CL} represents the inductive behavior of the current collectors in the cell and can only be observed at high frequency on the positive imaginary axis of the Nyquist plot. Resistor R_{CL} , also known as ohmic resistance models the resistance from collectors, binders, electrodes and electrolytes. The effect of these resistances can be observed on the Nyquist plot where the impedance crosses the real impedance axis. To model the solid electrolyte interface (SEI) a resistor R_{SEI} and constant phase element CPE_{SEI} in parallel are used. Lithium is consumed at the anode in an irreversible process, where a lithiated carbon and electrolyte reaction occurs to form a SEI layer. The SEI layer causes a decrease in capacitance and increase in resistance, it can be observed on the Nyquist plot at high to middle frequencies at the beginning of the compressed semi-circle.

Charge transfer resistance R_{CT} and double layer capacitance CPE_{DL} occurs in tandem from the accumulation of positive and negative electrolytes at the electrode/electrolyte interface. This phenomenon happens when an electrical load is applied to a cell because of an exchange of electrons at the electrode/electrolyte interface. One technique to estimate charge transfer resistance for a reaction is dependent on the concentration of the species involved in the reaction. It can be expressed by kinetic and limiting currents known as Koutecky-Levich analysis (2) [23].

$$R_{t,Li} = R_{t_{lim},Li} \left(1 + \frac{\bar{i}_{lim,Li}}{\bar{i}_{k,Li}} \right) \quad (2)$$

The ratio of $R_{t,Li}$ and $R_{t_{lim},Li}$ approaches unity as the kinetic current $\bar{i}_{k,Li}$ becomes very large at positive potentials. The charge transfer resistance can also be expressed by (3), where the resistance does not depend on the concentration of the chemical species. Charge transfer resistance for such system approaches zero at very positive potentials [23].

$$R_{t,Li} = \frac{1}{K_{Li} b_{Li} \exp(b_{Li} \bar{V})} \quad (3)$$

$$b_{Li} = \frac{\alpha_{Li} nF}{RT} \quad (4)$$

The charge transfer resistance can also be estimated when polarization depends solely on kinetics of the reaction in (1). Equation 5 is derived from Butler-Volmer equation and can be used when the cell is at equilibrium and the overpotential is small. Where i_0 is the exchange current density and is based off the concentrations of the electrolyte and the species of reactant, (6).

$$R_{t,Li} = \frac{RT}{nF i_0} \quad (5)$$

$$i_0 = FK_{Li} c_e^{1-\alpha} (c_{max} - c_s)^{1-\alpha} c_s^\alpha \quad (6)$$

Double layer capacitance can be estimated directly from the charge transfer resistance. Assuming charge transfer resistance and double layer capacitance operate as an ideal RC circuit, (7) relates the two by using the maximum frequency under the section of the Nyquist plot where these two phenomena occur. Both processes can be observed on the Nyquist plot at mid-low frequencies.

$$C_{dl} = 2\pi f_{max} R_{t,Li} \quad (7)$$

Diffusion is a mass transport phenomenon where charged and uncharged particles migrate to balance concentration differences created by electrochemical potential. The Warburg impedance coefficient can be express by (9) [33], where subscript o and r represent the diffusion and concentration of the oxidation and reduction of the species.

$$D_{Li} = \left(\frac{\frac{i_p}{\sqrt{v}}}{(2.68 \times 10^5) n^{\frac{3}{2}} C_o^0} \right)^2 \quad (8)$$

$$\sigma = \frac{RT}{(nF)^2 A \sqrt{2}} \left(\frac{1}{D_o^{1/2} C_o^b} + \frac{1}{D_r^{1/2} C_r^b} \right) \quad (9)$$

$$Y = \frac{1}{\sqrt{2}\sigma} \quad (10)$$

The diffusion coefficient for Li^+ ion is calculated assuming the intercalation process is fully reversible, using the cyclic voltammetry diffusion equation. Calculations are valid for temperature at 300°K and calculated using (8) [34]. The impedance caused by diffusion is produced at low frequencies and is expressed in terms of the Warburg coefficient (10).

2.2 Fitting Techniques

When fitting models to experimental data there are many approaches that can be used. The determination of what type of fitting routine that is needed depends solely on the proposed model for said experimental data. In this study we will discuss three common fitting techniques ranging from: linear least square fitting, nonlinear least square fitting, and finally complex nonlinear least square fitting. Complex nonlinear least square fitting is regarded as the most robust technique to fit EIS measurements and is used throughout this study.

Linear least square fitting is a common approach to fit data in statistical linear regression models. This technique typically uses vertical offsets to determine the difference between the output of the model and the actual data points at a specified measurement interval. This difference is known as the residuals, and linear least square fitting minimizes the residuals for all the data points throughout the model to determine the best coefficients. The basic formulation for linear least square fit problems can be seen in (11), for $n \in \{1 \dots N\}$ at the observed pairs (x_n, y_n) . [31]

$$y = ax + b \tag{11}$$

Nonlinear least square fitting is an unconstrained minimization problem, where similarly to the linear least square fitting the objective is to minimize the sum of residuals between the model and data points. A generalized form of a nonlinear least square fitting problem is shown in (12), where $\{f(x)\}$ is a nonlinear function.

$$\min_x = \sum_{i=1}^n f_i(x)^2 \quad (12)$$

To solve this nonlinear optimization problem many different approaches can be used, in this study we will discuss the use of Gradient and Hessian method. Gradient and Hessian method is a relatively simple approach that uses Hessian and gradient matrices to solve for optimal fit. The Gradient and Hessian method solves for a search direction by utilizing (13), where the Hessian can be approximated to further simplify to (14). This approximation is valid with the assumption that the model is a perfect fit for the data [35].

$$\nabla^2 f(x)p = -\nabla f(x) \quad (13)$$

$$\nabla F(x)\nabla F(x)^T p = -\nabla F(x)F(x) \quad (14)$$

This method has the downside of poor performance when the model is not an adequate representation of the system. When the residuals are large, the assumption that the model is a perfect fit becomes invalid leading to the poor performance.

Complex nonlinear least squared (CNLS) fitting is generally regarded as the most adequate method for fitting impedance data. The use of which expects the real and imaginary impedance measurements to satisfy Kramer-Kronig relations, see EIS Measurement and ECM Validations. With satisfying K-K relations CNLS estimates combined model parameters by simultaneously fitting the real and imaginary impedance spectrum.

The minimization function between the model and measured impedance data for CNLS is shown in (15). Where $Z(\omega|\mathbf{P})$ is the complex impedance model, calculated for frequency ω and a function of \mathbf{P} the vector of parameter values (9 elements). $Z(\omega)$ is the

measured impedance data and \mathbf{V} is a symmetric positive-definite variance-covariance matrix from the experimental stochastic errors. The minimization function simplifies to (16) under the assumption that \mathbf{V} is a diagonal matrix and residuals are uncorrelated [33].

$$S = (Z(\omega) - Z(\omega|\mathbf{P}))^T \mathbf{V}^{-1} (Z(\omega) - Z(\omega|\mathbf{P})) \quad (15)$$

$$S = \sum_{k=1}^N \left[\frac{(Z_r(\omega_i) - Z_r(\omega_i|\mathbf{P}))^2}{V_{r,k}} + \frac{(Z_j(\omega_i) - Z_j(\omega_i|\mathbf{P}))^2}{V_{j,k}} \right] \quad (16)$$

With the previously stated assumptions the real and imaginary components of impedance are fit simultaneously. Subscripts r and j represent real and imaginary components, while N is the number of data points.

Methods for solving CNLS fitting can be done using; Gauss-Newton, steepest decent, Levenberg-Marquardt, and downhill simplex method. Downhill simplex method only evaluates the objective function and does not require derivatives or inverse matrices. For these reasons downhill simplex method is a far more robust method and will be used to fit data in this study.

Simplex method is evaluated in $P + 1$ space by using a geometric figure called a simplex, where P is the number of parameters. The simplex is evaluated using a series of decision and operations to minimize a cost function. Operations to reconfigure the simplex include; reflection, expansion, contraction, etc. [36]. The utilizations of the CNLS requires initial parameters to solve, therefore having well estimated starting parameters can lead to fast-accurate data fitting.

2.3 Fitting Method for Proposed ECM

Electrochemical impedance spectroscopy data for all EIS measurements is fit to the proposed ECM using the simplex method. The simplex method as previously stated is an optimization algorithm, that uses functional evaluation to settle at a local minimum [32]. When using this algorithm defining constraints and initial parameters for element values will avoid local minima that are not regarded as logical outcomes. In this experiment, lower limits are set to zero or greater for all equivalent circuit elements; according to Gamry element values are generally regarded as positive values. The upper bounds for conditioning numbers on both constant phase elements are set to one, this corresponds to the well-known range for the condition number of a CPE element. Where zero reflects a resistor frequency response and one reflect an ideal capacitor frequency response.

The initial value Warburg diffusion element was estimated using (17) and (10), where the diffusion coefficient is $2e^{-15} \text{ m}^2/\text{mol}$. This value comes from the experimental study in [37] and is within known values for diffusion coefficient of the cathodic material, $LiMn_2O_4$.

Table 2 contains the values used to estimate the diffusion coefficient for the Li-ion pouch cell. This estimation assuming the cathodic material is the limiting factor for the diffusion reaction in the cell, with this assumption (9) simplifies to (17).

$$\sigma = \frac{RT}{(nF)^2 A \sqrt{2}} \left(\frac{1}{D_{Li}^{1/2} C_o^b} \right) \quad (17)$$

The initial value for the ohmic resistance can be estimated using the Nyquist plot, and a value of $1 \text{ m}\Omega$ is a sufficient estimate for all EIS measurements in this study. Having these two parameters well estimated, we use the fit of the first EIS measurement of each cell for

the final fitting procedures initial parameters, see Table 3. All following fits for each cell used the previously determined parameter values as initial parameter values for subsequent fits.

We use a sum of weighted errors χ^2 to evaluate the goodness of fit the model to the data see EIS Measurement and ECM Validations. Other characteristics of the fit being evaluated are the residuals and element errors. According to Gamry, more random the residuals about the actual data equate to a more accurate fit. Elements in the model shouldn't have errors larger than the value of that given element, fewer large element errors show the model is appropriate for the electrochemical processes occurring in the cell.

Table 2: Parameter values used to estimate value for diffusion coefficient of Li-ion pouch cell (Eq. 17)

Parameter	Description	Value
n	Number of electrons transferred per mol of reaction species	1
F	Faraday's constant	96500 $\frac{\text{Coulombs}}{\text{equivalent}}$
R	Universal gas constant	8.314 $\frac{\text{J}}{\text{mol K}}$
T	Temperature	300 °K
D_{Li}	Diffusion coefficient for Li ⁺ ion	$2e^{-15} \frac{\text{m}^2}{\text{s}}$
c	Li ⁺ ion concentration	2.29 $\frac{\text{mol}}{\text{m}^3}$
A	Area of electrodes	72 cm ²

Table 3: Initial Fitting Parameters for Simplex Method

<i>ECM Element</i>	<i>Initial Value</i>	<i>Lower Constraint</i>	<i>Upper Constraint</i>	<i>Units</i>
L_{CL}	50	0	N/A	nH
R_{CL}	1	0	N/A	mOhms
R_{SEI}	1	0	N/A	mOhms
CPE_{SEI}	30	0	N/A	$S \cdot s^n$
n_{SEI}	0.5	0	1	-
R_{CT}	0.001	0	1	Ohms
CPE_{DL}	1000	0	N/A	$S \cdot s^n$
n_{DL}	.5	0	1	-
W_{Diff}	0.1	0.001	1	$S \cdot s^{1/2}$

2.4 Summary

Presented in chapter 2 was the electrochemical process-based ECM used to fit EIS measurement. The electrochemical processes used to construct the ECM were outlined along with approaches to estimate their respective values. We use simplex method, a complex nonlinear least square fitting technique to fit the proposed model to experimental data. Finally, the fitting procedure and initial parameters for all fitted data is introduced.

CHAPTER 3 – CONTROLLED MECHANICAL DAMAGE WITH LOW C-RATE CYCLING

The experiment we discuss in chapter 3 investigates the short-term changes to the electrical response of the previously described cell after sustaining controlled mechanical damage and being subjected to low c-rate cycling. In this study a single cell was subjected to a hemi-spherical punch after establishing baseline EIS measurements. Three control cells were used to determine and characterize any trend changes in ECM parameter values to the indented cell. All cells in this experiment underwent identical cycling procedure and EIS measurements were performed at 0% SOC.

3.1 Method and Set-up

A four-electrode connection was used for the pouch cells in this study, two current carrying leads, one working sense, and one reference lead. The positive current carrying, and reference leads are connected to the positive electrode and the negative current carrying and working sense leads are connected to the negative electrode. Each Li-ion pouch cell was placed on the holder, where two pieces of copper compress each electrode separately. The current carrying leads are in direct contact with the top of each copper plate and fastened down with a washer and nut. Each copper plate also has a connection port for the reference and working sense leads respectively. Finally, to secure the cell and create consistent connection between the electrodes and copper plates a middle screw is fastened down between the two electrodes. The middle screw and a strap on the base of the holder secure the cell in place, ensuring it does not shift during testing and transportation.

The effect of mutual inductance is most prevalent at high frequencies. It is important to reduce the mutual inductance created by leads, [28] this can be accomplished by twisting lead pairs together and separating sense and current carrying lead pairs. Twisting sense leads together reduces magnetic field effects by decreasing the magnetic loop areas interacting with opposing wires. Also, opposite polarity voltages from adjacent magnetic loops cancel out, furthermore minimizing magnetic field effects. Separating current carrying leads from sense leads decreases the magnetic fields effect on opposing lead pairs by the inverse squared distance. When performing low impedance EIS measurements a change in configuration of sense and current carrying leads can cause phase shifts in identical cells. Reproducing the same wire configuration is crucial for obtaining reliable and repeatable results. In this experiment the sense leads were twisted together and taped in place to keep the number of twists the same throughout data collection. The current carrying leads are Gamry cables specially designed for connection with the Reference 30k Booster to minimize mutual inductance caused by high current. They were taped down to the table for consistency in data collection. Finally, the cell holder is positioned identically for each EIS measurement. The experimental set-up can be seen in Figure 4 and was not altered throughout the data collection process.

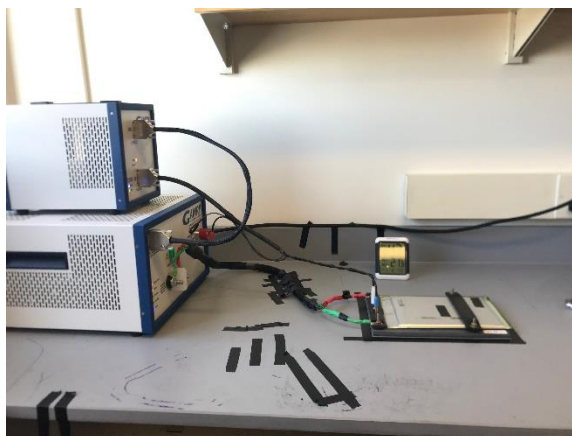


Figure 4: Li-ion pouch cell connection to Gamry 30k Booster for EIS measurements

Potentiostatic EIS was performed for a frequency range of 300 kHz to 10 mHz with excitation voltage of 10 mV. EIS was performed on the fully discharged cells (SoC \approx 0%) as a precaution for the unknown effects mechanical damage will cause on cells. The open circuit voltage for each cell was measured for 60 seconds prior to each EIS measurement, and the room temperature and humidity were recorded. The frequency range being studied is 2 kHz to 10 mHz, each EIS measurement performed on the pouch cells have impedance measurements at the same frequencies.

Cycling is done using constant current constant voltage charging, and constant current discharging. This technique supplies a constant current to the cell until the battery reaches a maximum threshold voltage. Followed by a constant voltage to the cell until the current reaches a minimum threshold value. The cells in this study are supplied 10% of capacitance current value until 4.1V, and then supplied a constant 4.1V until the current reaches 1% of the capacitance current value. Constant current discharging was done at 10% of capacitance value until the cell's voltage drops to 2.7 V. A thermocouple was attached to the middle of each cell prior to cycling and a relaxation period of at least 10 hours was used prior to EIS

measurements. It has been suggested in [1] that after a 4- hour relaxation period from electrical loading Li-ion batteries will experience little to no change in EIS measurements.

All cells went through initial characterization with low (1/10) C-rate cycling and impedance spectra measurements. Following the 5th cycle and ensuring consistency in the samples, we introduced controlled mechanical damage to cell 4. It was taken out of the cell holder and a hemi-spherical punch test was performed at the geometric center, see Figure 5. The mechanical deformation was done following the findings in [28]. A 57 mm hemispherical punch was used a rate of 1 mm/min to a depth of 2.8 mm. Voltage, depth and force versus time was recorded throughout the punch. All four cells were cycled 10 additional times to investigate the short-term effects of mechanical damage on the frequency response.

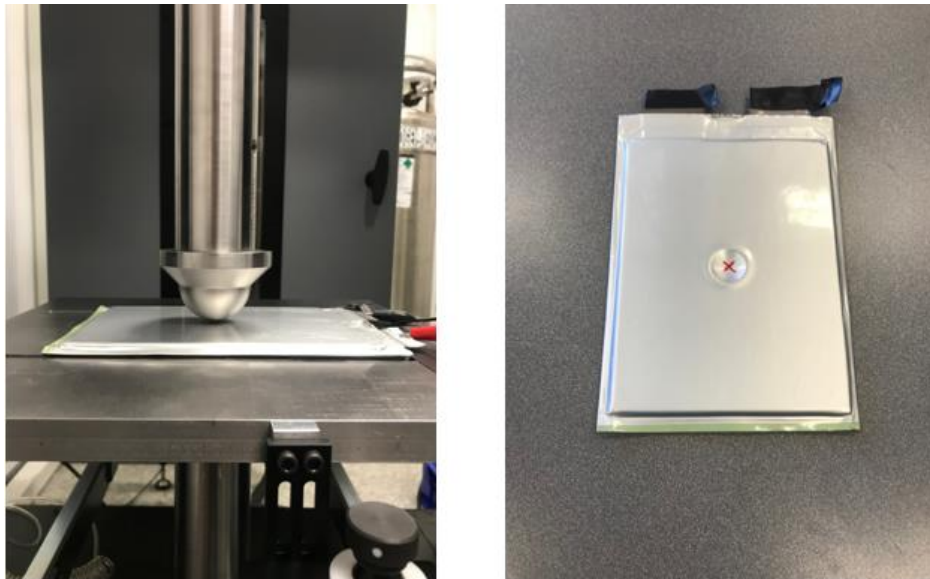


Figure 5: Punch test set-up and final 2.8-mm indentation

3.2 Results

The room temperature during EIS measurements was between 23.4 and 22.3 °C, and the humidity was measured to be between 50 and 43%. Impedance measurements, fitted model, and K-K transforms are shown on the Nyquist and Bode plot Figure 6. These plots show the ECM used for data fitting accurately predicts the frequency response of these Li-ion pouch cells. The quality of the fitted data can be seen in Figure 6, we note that the errors were less than 10^{-4} for all fitted data. Another notable attribute of the fitted data is that the error is minimal for many of the circuit elements. The model proposed in this study follows criteria acceptable for estimation of the frequency response.

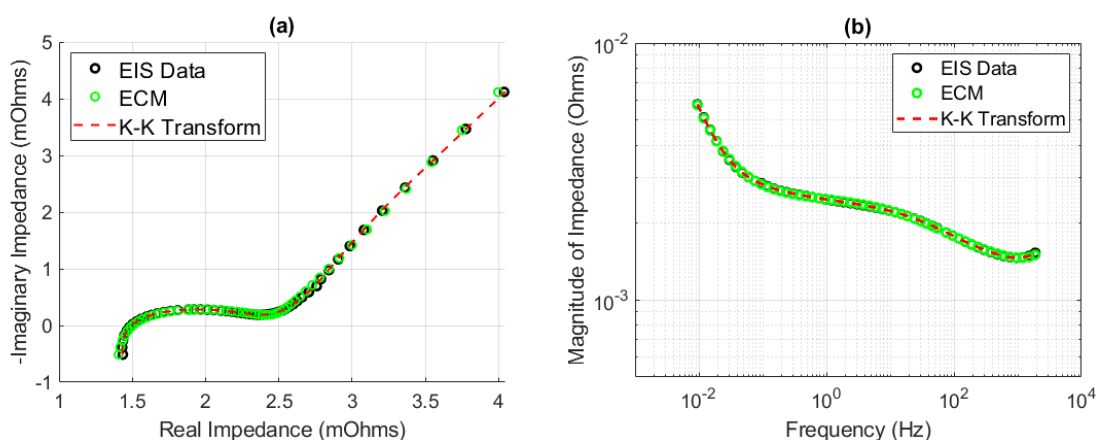


Figure 6: Experimental data fitted to the proposed ECM and K-K transforms (a) Nyquist (b) Bode

Following the 5th cycle, cell 4 underwent controlled mechanical damage in the geometric center of the cell as described in section 3.1. Voltage was essentially constant at 2.862 V, showing that there was no electrical short in the cell. All four cells were cycled 10 additional times to investigate the short-term effects of mechanical damage on the frequency response. Figure 7 and Figure 8 shows the trends in the ECM parameter values throughout low c-rate charge/discharge EIS measurements. These figures indicate that there is no substantial difference in ECM parameters between the indented and intact cells.

It can also be seen that the model produces similar trends for each element. We note that the ohmic resistance in Figure 7b varies by at most 1.4 m Ω for every cell, this can be attributed to connection with the potentiostat. Low-impedance measurements for this region are more susceptible to variation because of extreme difficulty in reproducing the exact same connection.

One element in the model that is interesting to note, is the CPE element modeling the solid electrolyte interface. Figure 7d and 7e show the trends in the CPE elements parameters, Q and n. The indented and intact cell show no difference in trend changes but do follow a known process in electrochemistry. The increase Q value for SEI layer is trending upward showing signs of ageing in the cell [27]. The parameter values in Fig. 8a and 8b, which model the double layer capacitance show a unique correlation with the voltage throughout the charge/discharge EIS measurements. Looking at Figure 8d, the voltage for EIS measurements starts at 3 volts and after two to three cycles becomes nearly constant for each cell. The same trend is seen for the double layer capacitance phenomena and suggests that the cell voltage of Li-ion pouch cells has a direct relationship with the double layer capacitance.

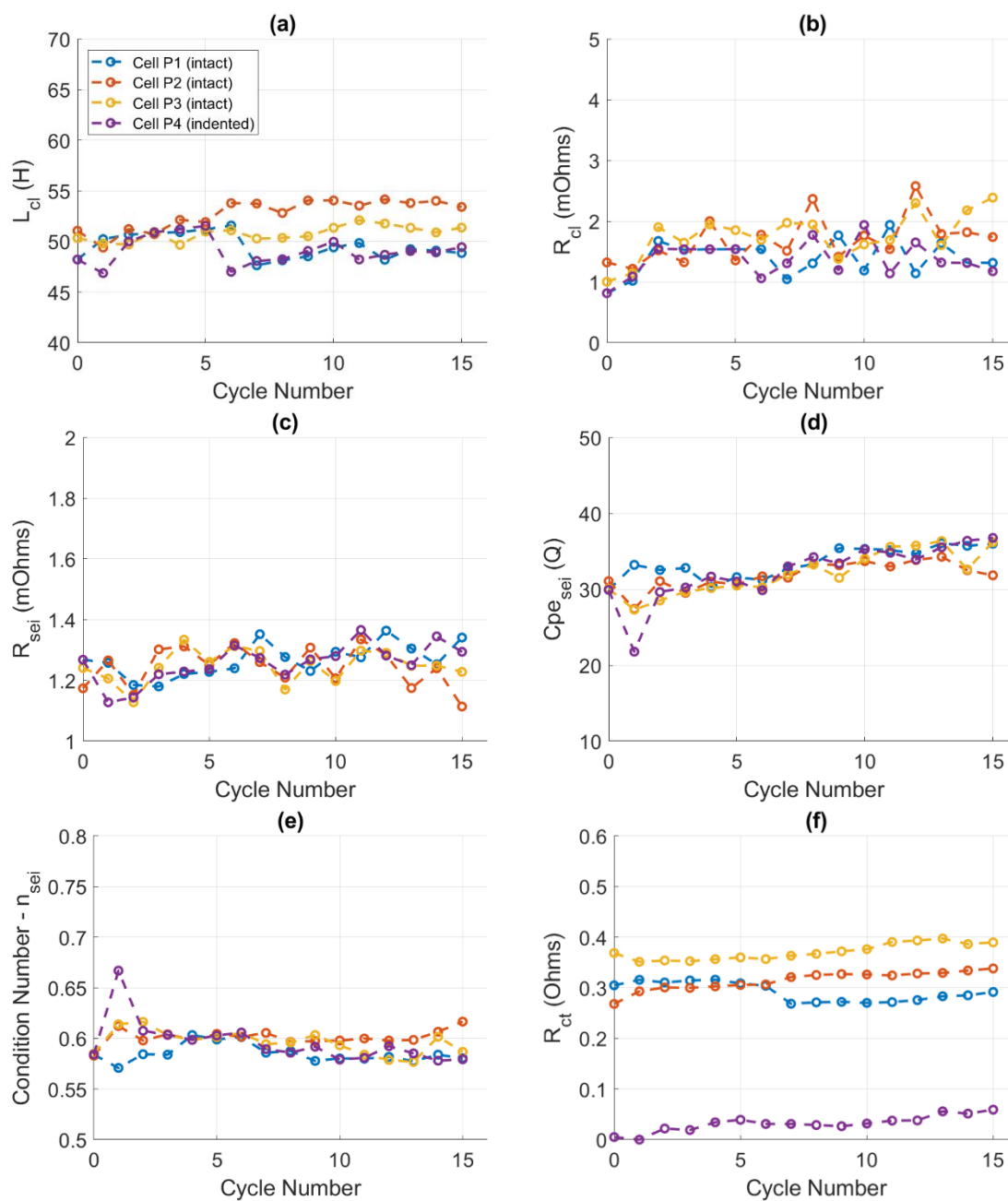


Figure 7: Trend changes of ECM parameter values throughout charge/discharge EIS measurements: (a) inductance, (b) ohmic resistance, (c) solid electrolyte interface resistance, (d) Q_{CPE} of the SEI layer, (e) conditioning number of the SEI layer and (f) charge transfer resistance

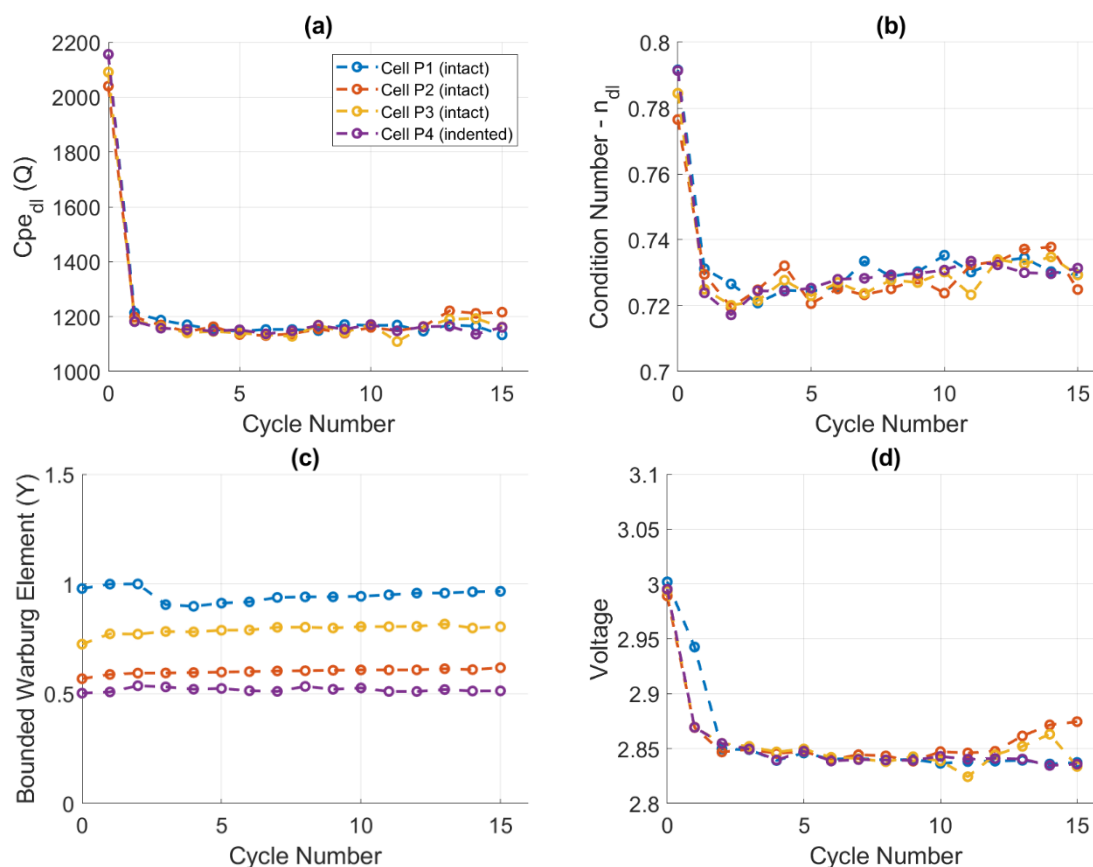


Figure 8: Trend changes of ECM parameter values throughout charge/discharge EIS measurements: (a) double layer Q_{CPE} , (b) double layer conditioning number, (c) bounded Warburg element and (d) OCV

3.3 Summary

Discussed in chapter 3 was the methods and results of low c-rate cycling after a Li-ion pouch cell was subjected to a hemi-spherical punch. Following the 5th cycle cell 4 was subjected to controlled mechanical damage, then cycled 10 additional times. This study showed that there was no substantial difference between the mechanically indented and intact cells. These results suggest that if a Li-ion pouch cells sustains mechanical damage and no immediate change in the electrical response is seen than it can continue to be cycled.

CHAPTER 4 – STEP INDENTATION WITH HEMI-SPHERICAL PUNCH

In this chapter, we examine the change in ECM parameter values throughout an indentation process. One cell is subjected to indentation from a hemi-spherical punch at specified depth intervals, followed by EIS measurements. This procedure captures the evolving ECM parameter values as depth of the mechanical damage is increased. Two cells are used as controls establishing a baseline response to successive EIS measurements. All cells in this experiment were cycled and at 0% SOC prior to indentation and EIS measurements.

4.1 Method and set-up

Step indentation was performed on cell 4, the previously indented cell. Following a similar procedure, using a 57 mm hemi-spherical punch at a rate of 1 mm/min. The cell was indented on the opposite side at 39.15 mm from the bottom and the geometric center of the width, see Figure 9. During this study temperature, voltage, depth, and force was recorded. EIS measurements were taken prior to indentation and following indentation intervals. The time between indentations was twenty minutes, with a ten-minute rest period after mechanical deformations followed by EIS measurements. The cell was indented at intervals; 2, 2.4, 2.6 mm followed by 0.1 mm steps until an electrical short occurred.

The cell was connected to the holder and Gamry instruments throughout the indentation and data collection process. EIS measurements were collected using a 10 mV excitation voltage and were performed at a frequency range of 300 kHz to 100 mHz. The cell was connected using a four-electrode connection as previously stated in the charge/discharge experiment and positioning of the experimental set-up was not altered during indentation. Connection to the cell holder and Gamry 30k Booster was done by rotating the cell 180°, see Figure 9. The frequency range being studied was 2 kHz to 100 mHz.

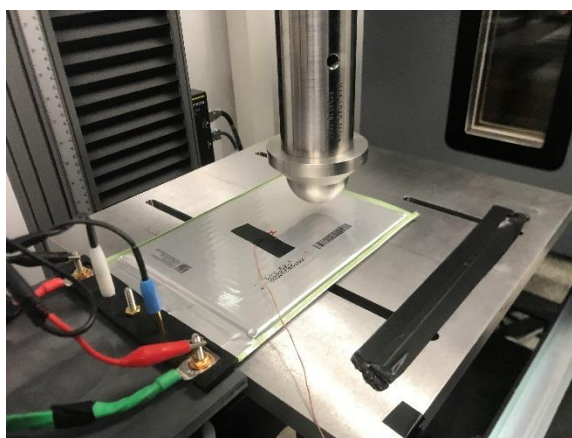


Figure 9: Step indentation set-up and connection to Gamry 30k booster for EIS measurements

4.2 Results

The fitting procedure for the following results is the same used for section 3.2. Cell 4 was incrementally indented until an electrical short occurred at 4-mm, and two cells were used as controls. The open circuit voltage (OCV) of cell 4 dropped with every successive EIS measurement following mechanical damage intervals. Voltage for cell 4 started at 2.837 V and fell to 2.780 V prior to the interval that caused an electrical short. The total drop in voltage for this cell was 5.724 mV. Control cell 1 had a starting voltage of 2.853 V and a final voltage of 2.783 V, while control cell 2 had a starting voltage of 2.863 V and a final voltage of 2.788 V. The total decrease in voltage for the control cells are 7.010 mV and

7.510 mV respectively. The rate of voltage drop is higher for both control cells and can be verified by the slopes in Figure 10f. Note control cell 1 underwent one less EIS measurement and if extrapolated along the existing trend, it would show a larger drop in voltage than presented.

The following data presented in Figure 10 and Figure 11a – Figure 11e are the ECM parameter value changes throughout the control experiments and step indentation. To capture the depths and time intervals for this experiment, voltage change is used for the independent variable. During the step indentation change in voltages encompasses the depth of the hemi-spherical punch and the time interval between EIS measurements. For the control cells the voltage encompasses strictly the time interval between EIS measurements. This means the only external influence on cell 4 is the indentation depth and any major changes in ECM parameter values can be attributed directly to punch depth.

It can be seen in Figure 10a, 10b, 10d and Figure 11a – Figure 11e that all ECM parameter values have similar trend changes. The values for all such elements start at the same magnitude and none of the stated elements vary greatly from the experimental control cells. It must be noted the charge transfer resistance in cell 4 has a single starting point that is inconsistent with the following parameter values, see Figure 11b. After the first inconsistency, the charge transfer resistance value retreats and forms a trend reminiscent of the control cells. For this reason, the inconsistency is treated as an outlier and not an indication of mechanical damage.

The most interesting of ECM parameter to note is the resistor element modeling solid electrolyte interface, see Figure 10c. The SEI resistance begins to increase following four EIS measurements for all cells in this study. It is apparent by viewing Figure 10c that cell 4's electrical response changes and the parameter values begin to rapidly increase compared to the controlled cells. This distinct difference between the damaged cell and the control cells is a clear indication that the cells characteristics have changed.

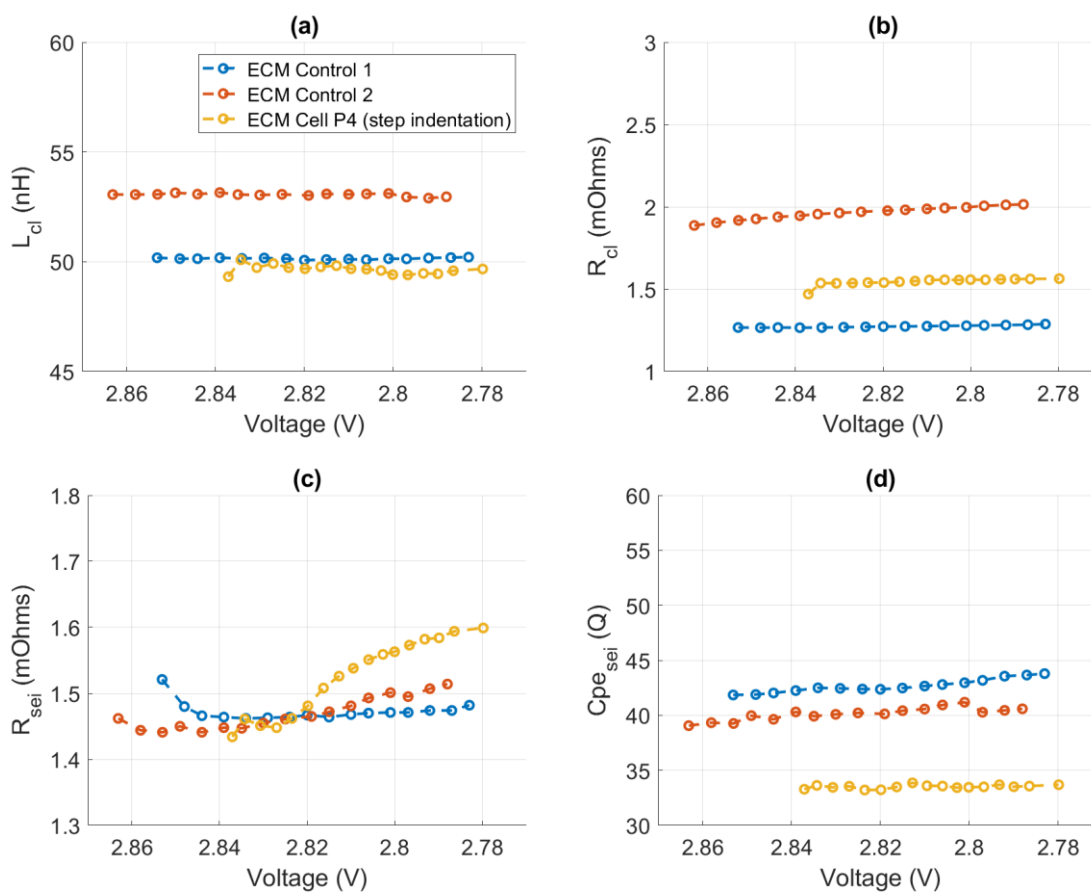


Figure 10: Trend changes of ECM parameter values throughout step indentation and control cell EIS measurements: (a) inductance, (b) ohmic resistance, (c) solid electrolyte interface resistance and (d) Q_{CPE} of the SEI layer

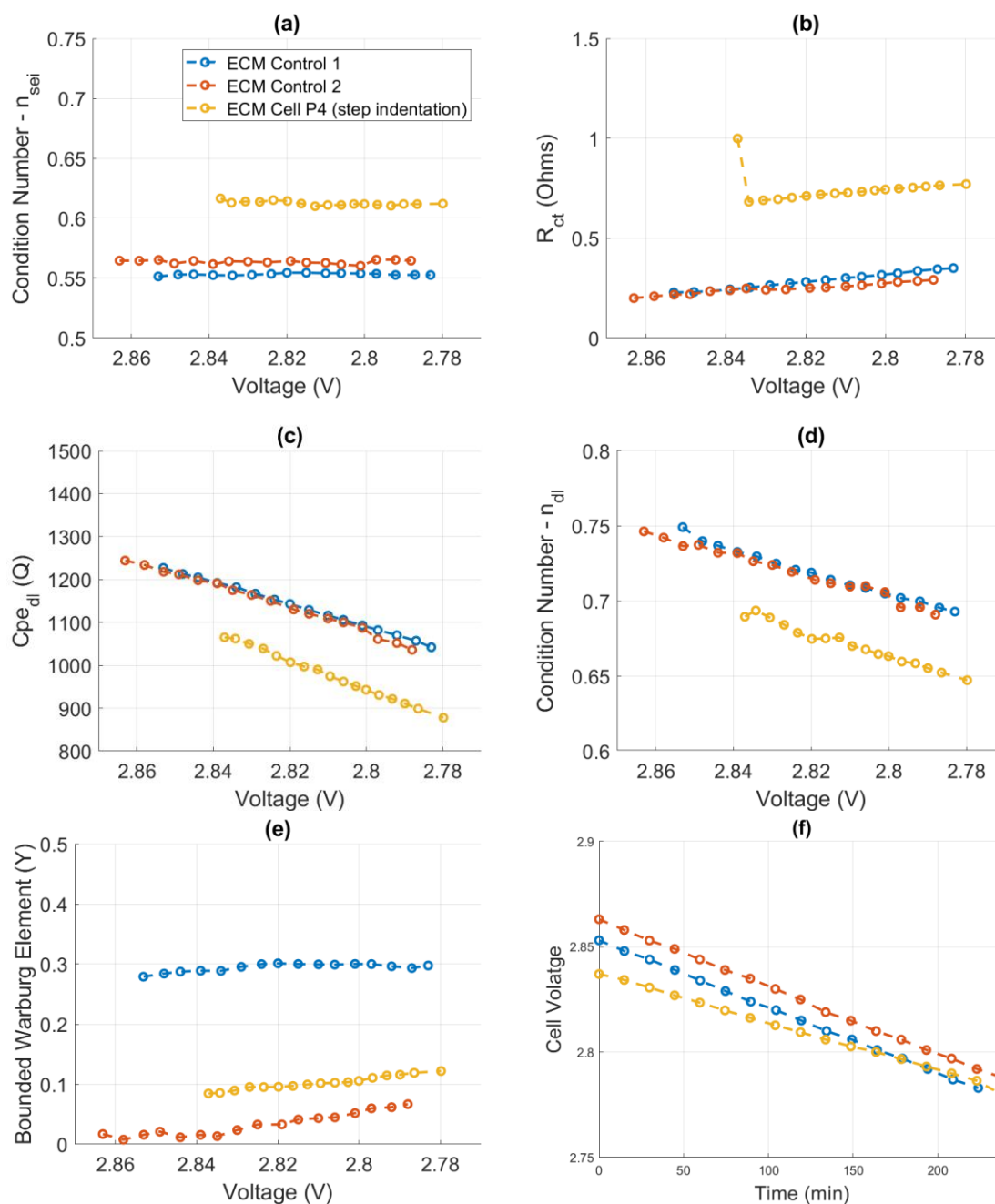


Figure 11: Trend changes of ECM parameter values throughout step indentation and control cell EIS measurements: (a) conditioning number of the SEI layer, (b) charge transfer resistance, (c) double layer Q_{CPE} , (d) double layer conditioning number, (e) bounded Warburg element and (f) OCV

The high and middle frequency regions for this experiment have been isolated as the region where the impedance spectrum is most affected by mechanical damage. Figure 12 presents the force versus displacement values throughout step indentation. The force values throughout step indentation experience vertical drops, this is the period where relaxation from mechanical damage occurs and EIS measurements are collected. During these time periods indentation depth is constant. The force applied during indentation periods experience no drop in force and suggest that the internal structure of the cell has not failed, see Figure 12. Figure 13a, 13b, 13d and Figure 14a - 14e present the ECM parameter values vs indentation depth of the hemi-spherical punch. All these trends do not indicate a distinct depth for when the batteries characteristics begin to deviate, except for the solid electrolyte interface resistance and double layer capacitance, see Figure 13c and Figure 14c.

First, we will address the double layer capacitance, as previously stated in 3.2 Results and can be seen throughout this study the double layer capacitance follows an identical trend to the voltage, see Figure 14c and 14f. Solid electrolyte interface resistance has been the key ECM parameter value in this experiment that has experienced a noticeable qualitative difference from the control cells. For this reason, it is extremely interesting to note that after a depth of 2.6 mm the SEI resistance begins to rapidly increase until an electrical short occurs. This suggests that after a critical depth the Li-ion pouch cells electrical response begins to change.

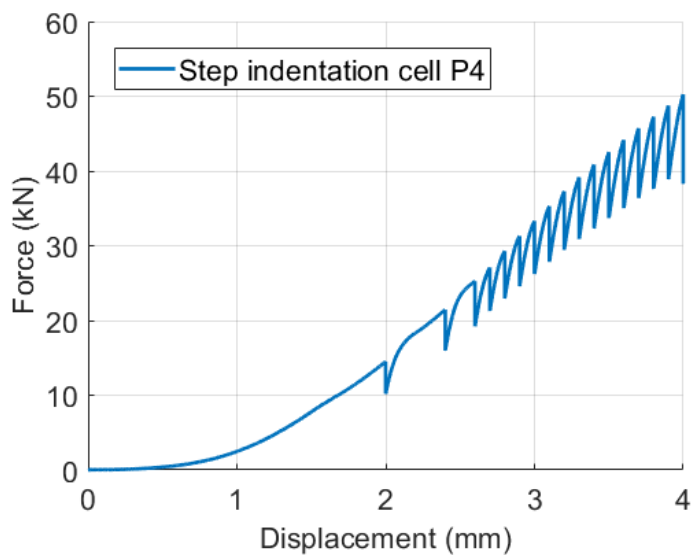


Figure 12: Force vs displacement during step indentation

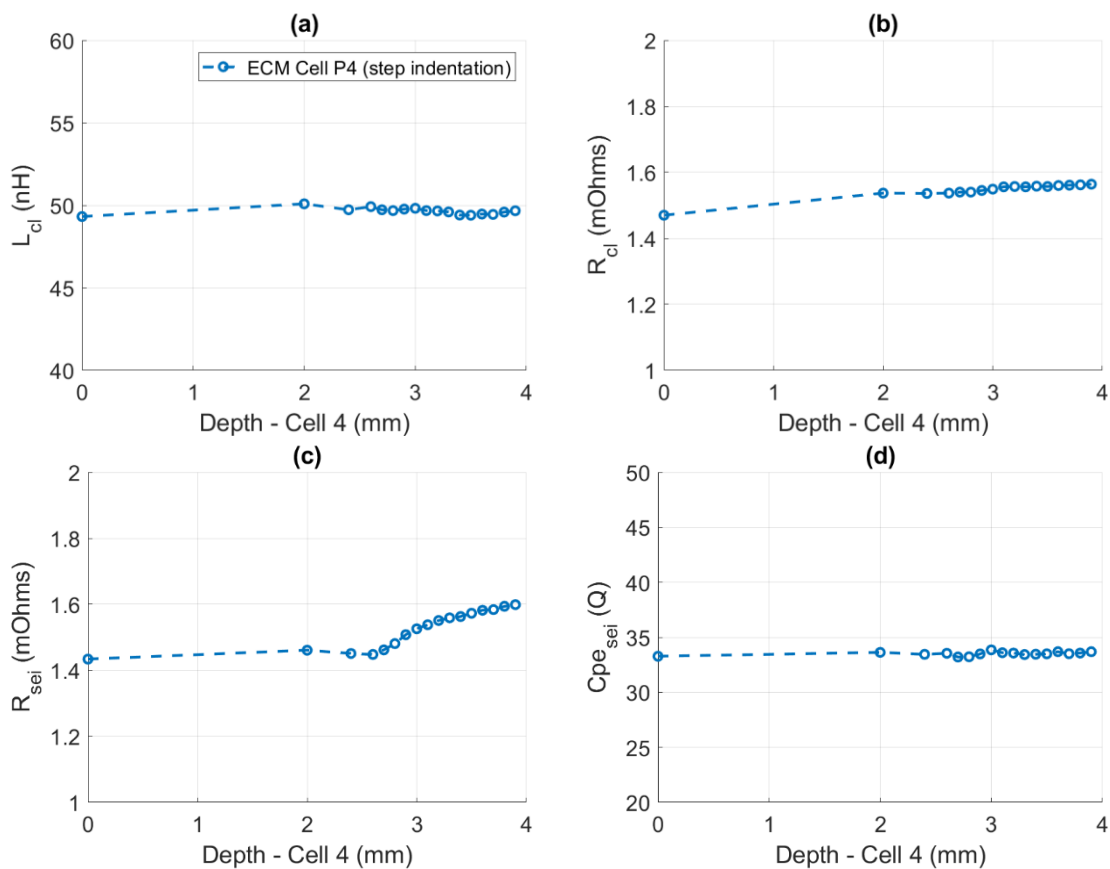


Figure 13: Trend changes of ECM parameter values vs depth throughout step indentation EIS measurements: (a) inductance, (b) ohmic resistance, (c) solid electrolyte interface resistance and (d) Q_{CPE} of the SEI layer

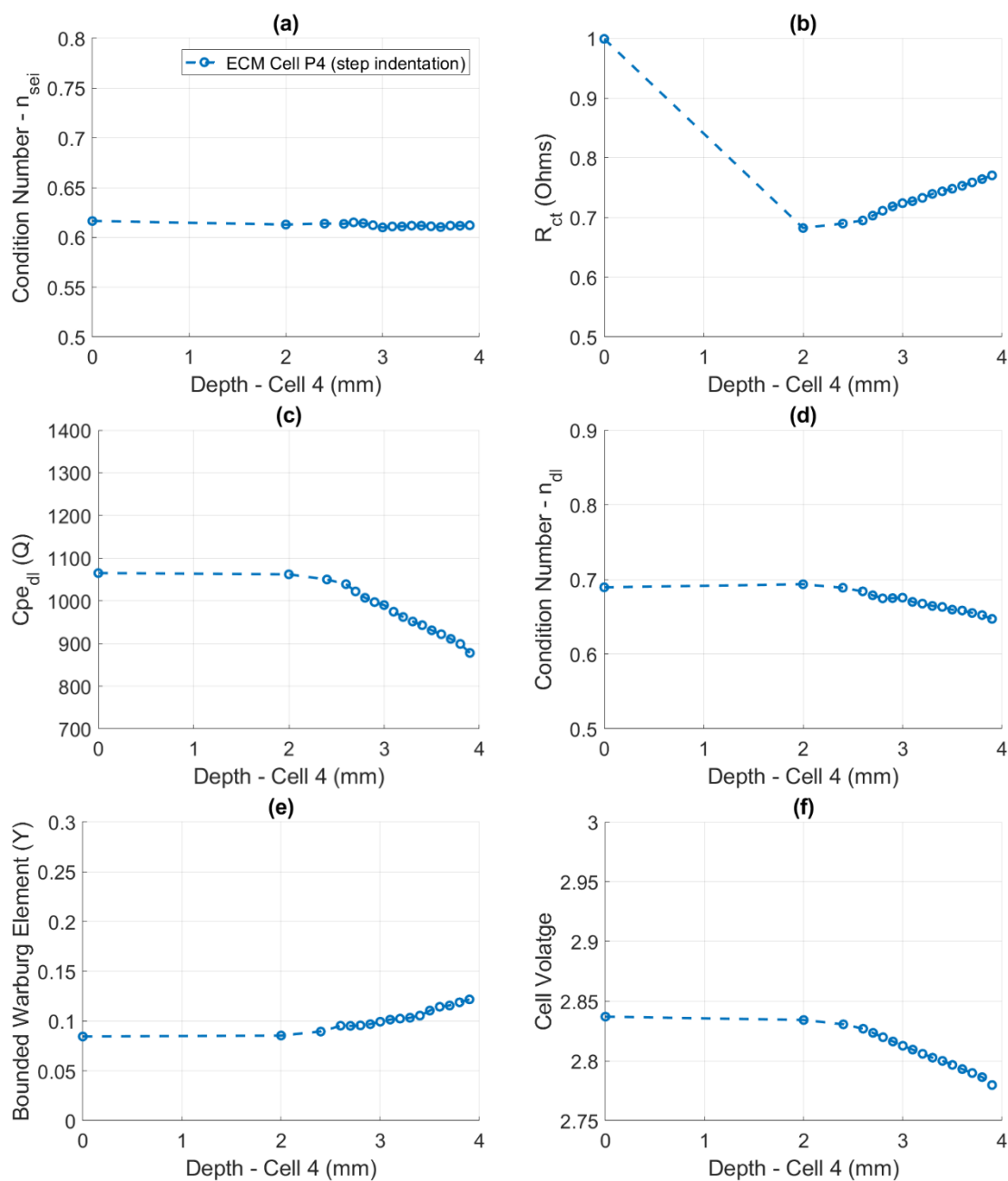


Figure 14: Trend changes of ECM parameter values vs depth throughout step indentation EIS measurements: (a) conditioning number of the SEI layer, (b) charge transfer resistance, (c) double layer Q_{CPE} , (d) double layer conditioning number and (e) bounded Warburg element and (f) OCV

4.3 Summary

The effects on the electrical response of Li-ion pouch cells subjected to incremental indentation was discussed in chapter 4. It was shown that high to middle frequency ranges of the impedance spectrum are the most effected by the applied hemi-spherical punch. This region on the impedance spectrum is modelled by SEI resistance and capacitance. The changes to the ECM parameter value trend began after 2.6 mm, see Figure 13C. These results suggest that if mechanical damage is severe enough an immediate change to a LIB electrical response can be observed.

CHAPTER 5 – STEP MECHANICAL THREE POINT BENDING

The experiment discussed in chapter 5 explores the effects of three-point bending on the previously described Li-ion pouch cells. In this experiment one cell was subjected to an ideal three-point bending scenario and the cells vertical geometric center was mechanically damaged in intervals as previously done in chapter 4. In identical fashion EIS measurements were taken between depth intervals to investigate the evolution of ECM parameter values. Three cells were used as controls. All cells in this experiment were cycled and a 0% SOC prior to indentation and EIS measurements.

5.1 Method and set-up

Three-point bending was performed on cell 3 following a charge/discharge cycle. Three-point bending was done using a center beam with a 15.60 mm radius and support beams with a 15.85 mm radius. Cell 3 was laid at the center of the support beams spaced 40 mm apart, see Figure 15. The force, displacement, and voltage were measured throughout mechanical damage. Following a similar procedure as step indentation EIS measurements were taken intermittently, and a relaxation period after mechanical damage of 10 minutes was used prior to EIS measurements. The center of cell 3 was intermittently displaced to the following depths: 1,2,4,8,10 and 12 mm. The cell was connected to a modified version of the previously described cell holder. The frequency range studied for three-point bending was 2 kHz to 100 mHz. Sense and working leads were secured in place to minimize external influences from wires shifting during three-point bending. A LVDT sensor was attached to the Instron to verify displacement measurements.

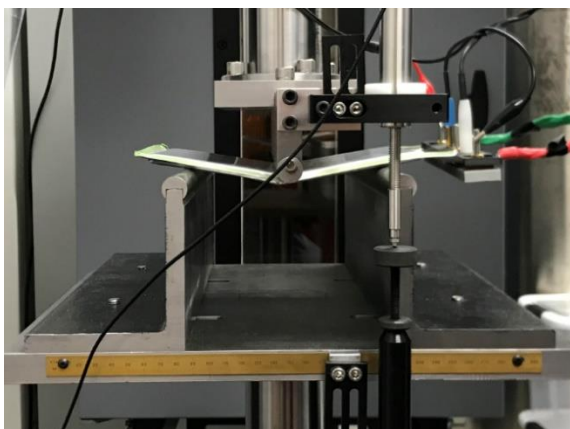


Figure 15: Three-point bending set-up and connection to Gamry 30k booster for EIS measurements

5.2 Results

The fitting procedure for the following experimental results are as stated for previous experiments in this study. Voltage trends for the additional control cell and cell that underwent three-point bending are identical to the stated trend in section 4.2. The starting voltage for cell 3 prior to three-point bending was 2.801 V and fell to 2.782 V, the total drop in voltage was 1.895 mV. Starting voltage for control cell 3 was 2.833 V and the final voltage was 2.806 V, with a total drop of 2.664 mV. This is consistent with the previous experiment where mechanically damaged cell had a lower drop in voltage than the intact control cells, and verifiable by viewing Figure 17f. Experimental data in Figure 16 and Figure 17a – Figure 17e for three-point bending are presented identically to that in 4.2 Results. The ECM parameter values in Figure 16b, 16d and Figure 17a – 17Figure 17e show no substantial trend changes in ECM parameter values between control and mechanically damaged cells.

The ECM trend changes most interesting to note are the inductance produced by current carrying leads and solid electrolyte interface resistance. The trend for the inductance is shown in Figure 16a, there is a clear difference between the cell undergoing three-point

bending and all control cells. Control cells show that an intact cell has a constant parameter value for all voltages presented. Cell 3, being subjected to three-point bending begins with a constant inductance and then rapidly increases as the depth mechanical damages increases. The solid electrolyte interface resistance in cell 3 shows a similar difference in trend where the control cells are slightly increasing following an initial drop. The mechanically damage cell increases more rapidly throughout three-point bending, see Figure 16c.

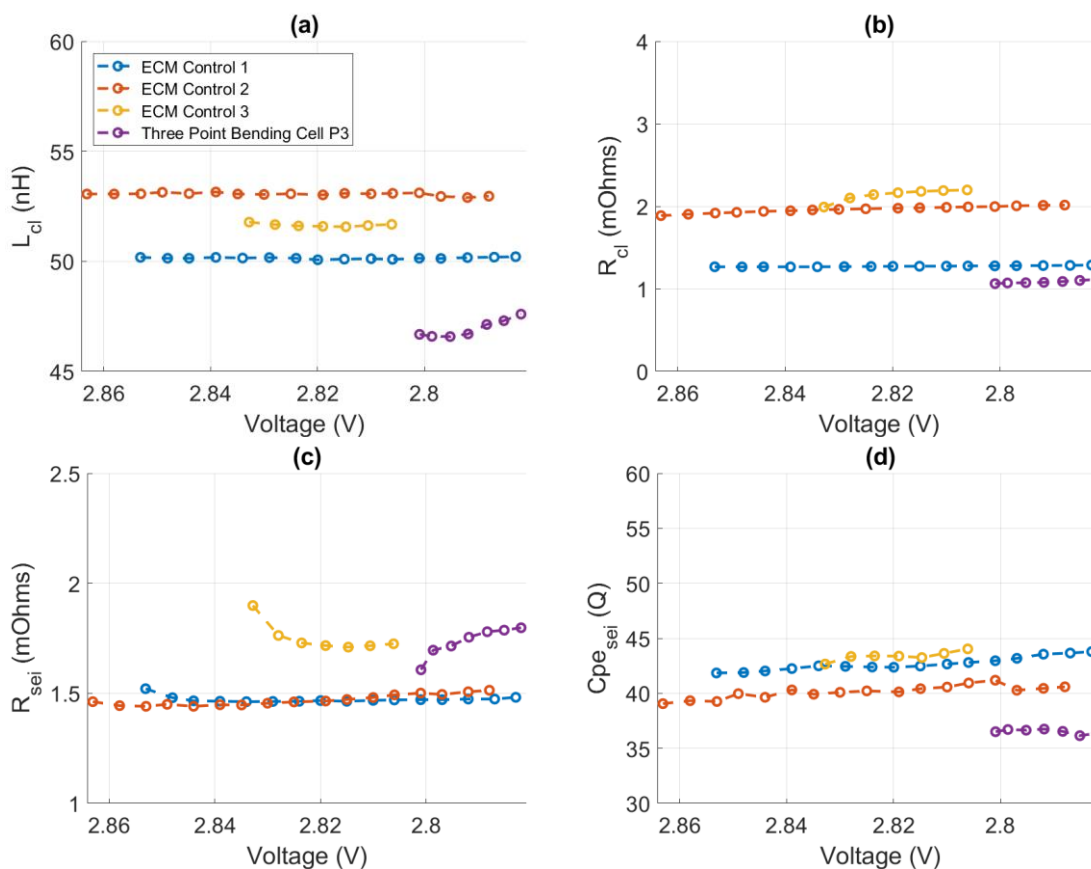


Figure 16: Trend changes of ECM parameter values throughout three point bending and control cell EIS measurements: (a) inductance, (b) ohmic resistance, (c) solid electrolyte interface resistance and (d) QCPE of the SEI layer

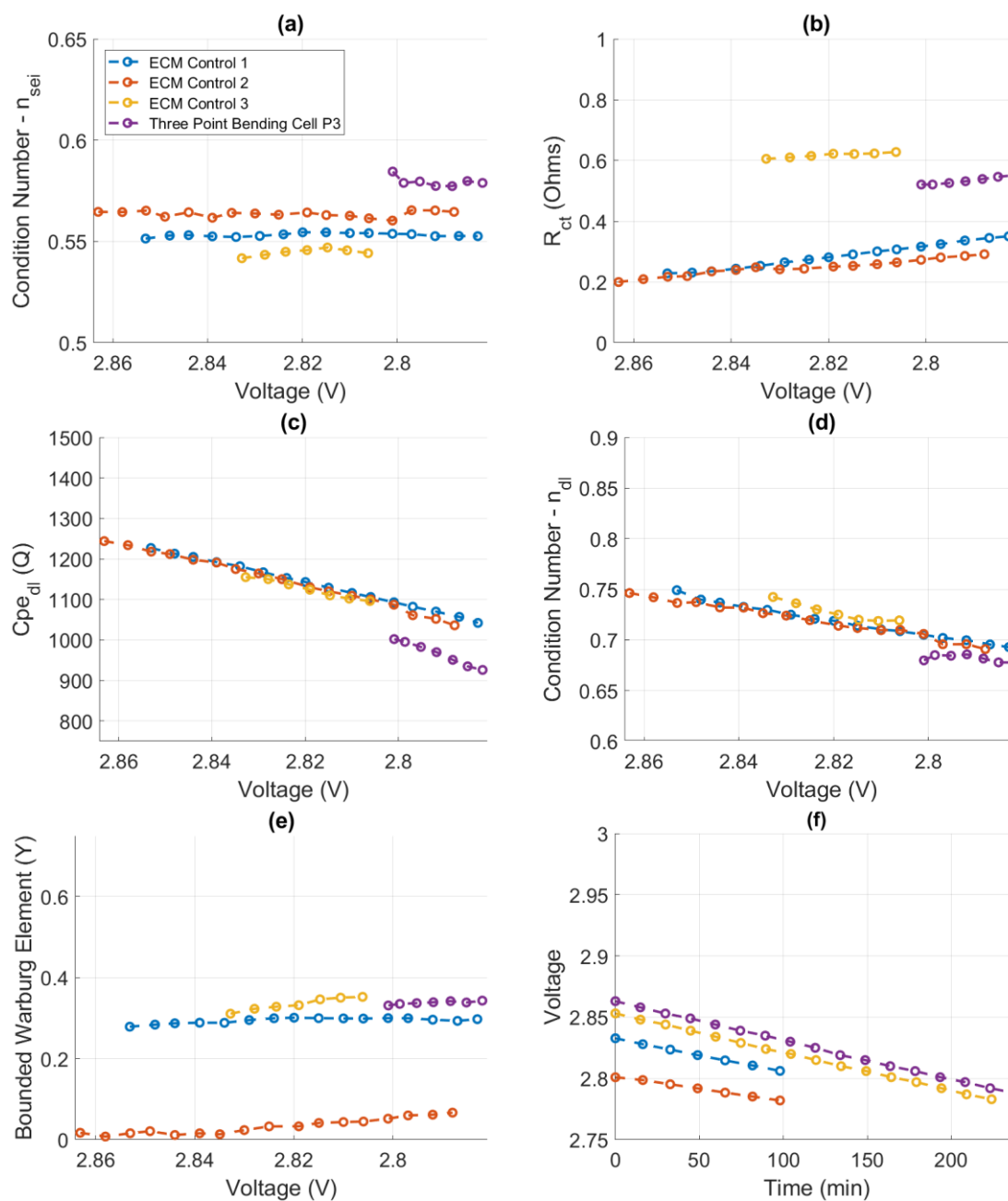


Figure 17: Trend changes of ECM parameter values throughout three point bending and control cell EIS measurements: (a) conditioning number of the SEI layer, (b) charge transfer resistance, (c) double layer Q_{CPE} , (d) double layer conditioning number, (e) bounded Warburg element and (f) OCV

We have established through qualitative reasoning that frequency regions of the impedance data that are most affected are the inductance caused by current collectors and the SEI resistance. Figure 18 presents the force vs depth during three-point bending, and it shows a decline in force at 2.63 mm and continues to drop throughout the experiment. This is very interesting to note because it suggests that layers of the cells internal structure may have failed. Figure 18 shows vertical drops in force, this is the period where relaxation from mechanical damage occurs and EIS measurements are collected. For these time periods indentation depth is constant.

There is more evidence to support the Li-ion pouch cell's physical and electrical characteristics have altered at this depth, see Figure 19a and 19c. Both the inductance and SEI resistance show a change in trend between 2 and 4 mm, this is the same depth where the original drop in force is observed. The inductance is nearly constant and immediately following the decline in force inductance begins to increase for every subsequent EIS measurement. A similar trend can be seen in the element modeling SEI resistance, where resistance starts to increase and following the critical depth the SEI resistance rate of change declines.

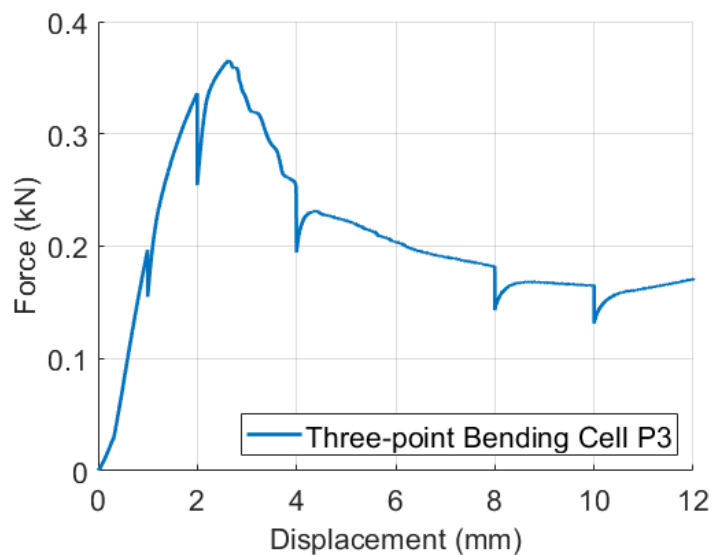


Figure 18: Force applied vs displacement of cell 3 during three-point bending

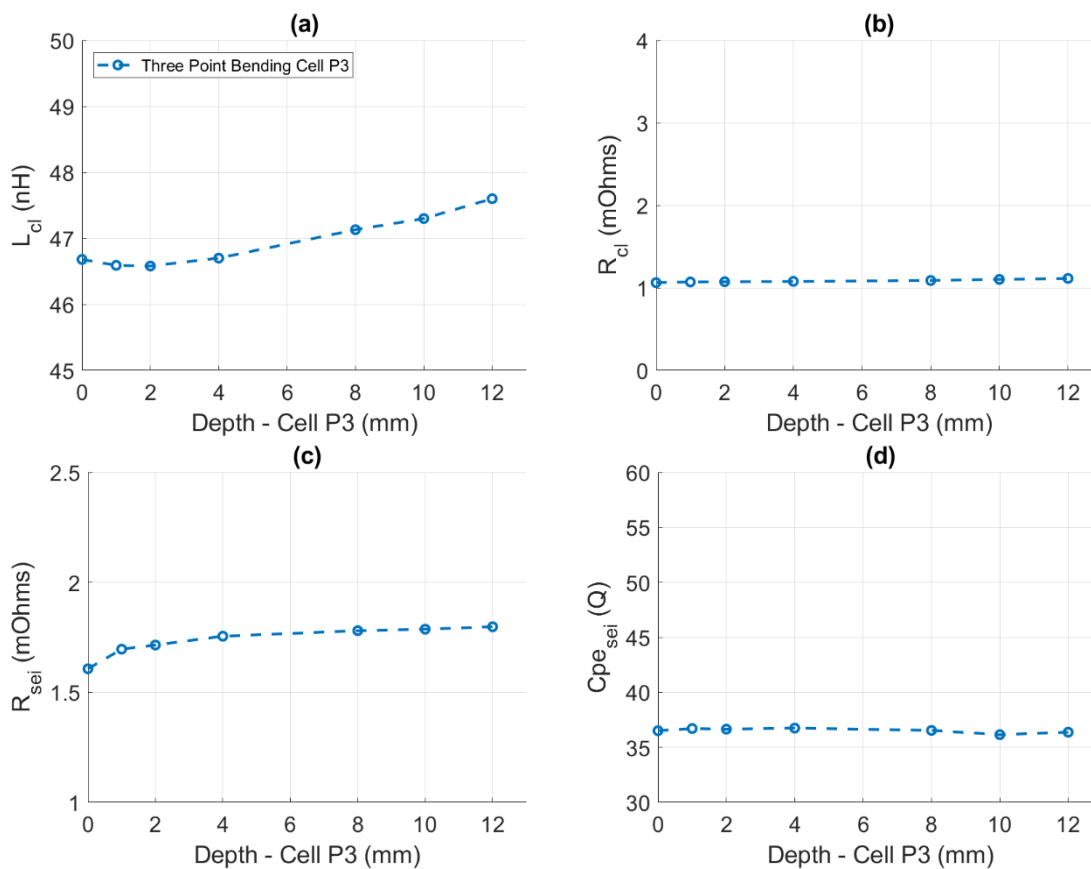


Figure 19: Trend changes of ECM parameter values vs depth throughout three point bending EIS measurements: (a) inductance, (b) ohmic resistance, (c) solid electrolyte interface resistance and (d) Q_{CPE} of the SEI layer

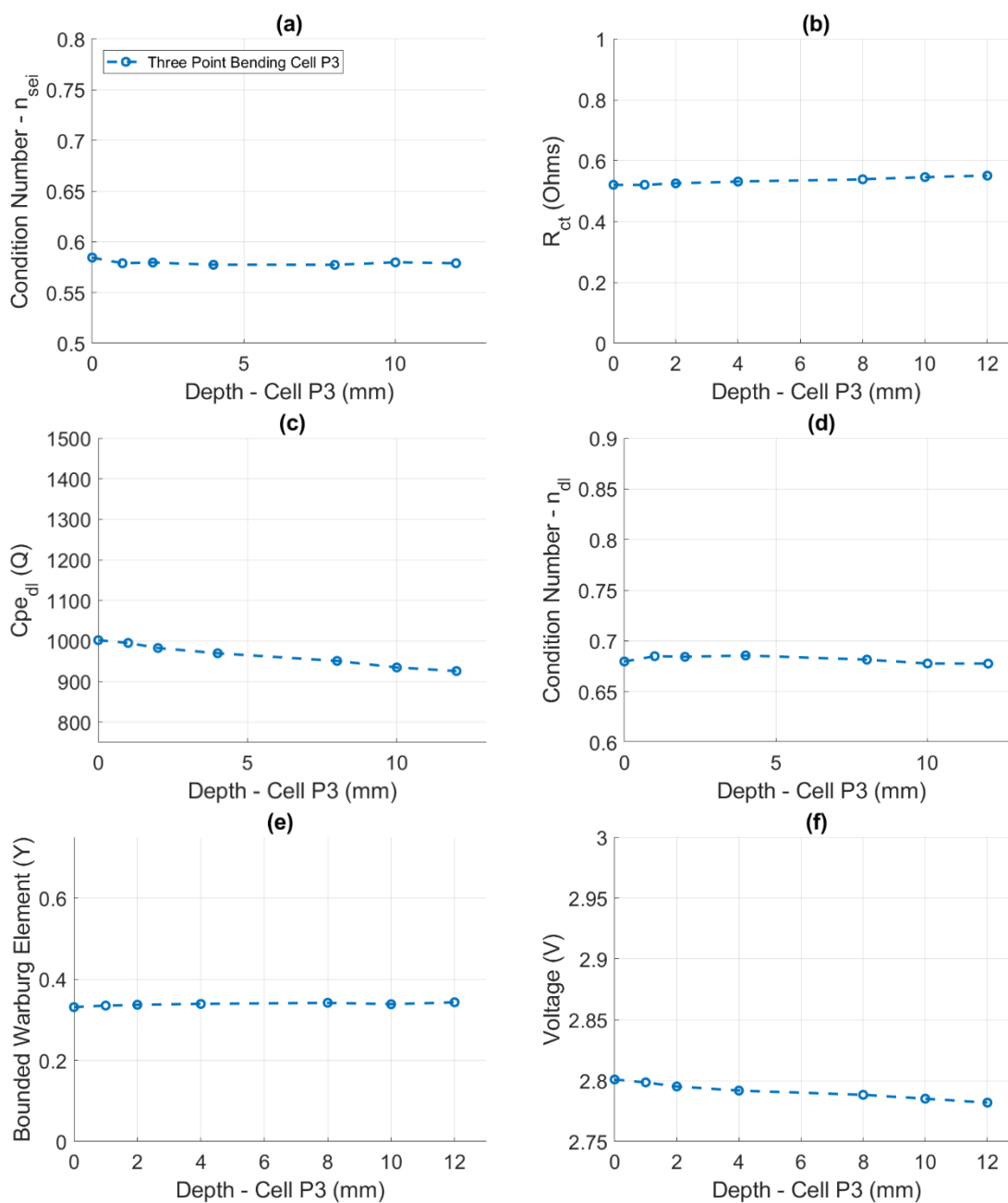


Figure 20: Trend changes of ECM parameter values vs depth throughout three point bending EIS measurements: (a) conditioning number of the SEI layer, (b) charge transfer resistance, (c) double layer Q_{CPE} , (d) double layer conditioning number (e) bounded Warburg element and (f) OCV

5.3 Summary

In chapter 5, a single Li-ion pouch cell was subjected to an ideal three-point bending scenario and incrementally damaged. This experiment revealed a force drop during mechanical damage occurring at 2.63 mm. This force drop was shown to be directly correlated with changes to ECM parameter values in the current collector inductance and SEI resistance. The results of this experiment suggest that signs of mechanical damage can be observed in the high to middle frequency range of the impedance spectrum.

DISCUSSION AND CONCLUSION

This study presented findings from three separate experiments where Li-ion pouch cells were subjected to controlled mechanical damage to investigate the effects on the electrical response. The three experiments include low c-rate cycling with a hemi-spherical indentation, hemi-spherical step indentation and ideal three-point bending. To model the electrical response of the cells in this study an electrochemical process-based ECM was proposed. All cells in this study were at 0% SOC when mechanically damaged and EIS measurements were carried out. The temperature and humidity conditions were similar for all EIS measurements.

Investigating the short-term effects of mechanical damage on the electrical response of Li-ion pouch cells was done using four cells. The four cells were cycled 5 times prior to one cell being mechanically damaged with a 57 mm hemi-spherical punch. Following the mechanical damage all cells were cycled 10 additional times. The results of this study showed no difference in ECM parameter value trend changes between the indented and intact cells. The ECM parameter trends do show signs pointing to ageing and capacity fade, see 3.2 Results. Results of this study suggest that if a LIB sustains mechanical damage and no immediate change to the ECM parameter values is detected then it can continue to be cycled.

Following the investigation into short-term effects of mechanical damage, the previously damaged cell was indented intermittently and EIS measurements were taken between indentation depths. Two cells were used as controls and EIS measurements were taken at the same time intervals as the indented cell. The qualitative results of this experiment show that the SEI resistance began to rapidly increase following an indentation depth of 2.6 mm. The results of this experiment do not show a specific depth at which ECM parameter values will change, because this cell had been indented in the previous experiment. These do however suggest, that detection of mechanical damage in Li-ion pouch cells can be done by examining the high to middle frequencies of the impedance spectrum.

The final experiment performed to investigate the effects of mechanical damage on the electrical response of Li-ion pouch cells, was to subject a single cell to an ideal three-point bending scenario. The support beams were separated by 40 mm and the cell was deflected in the center. The data collection procedure was identical to the step indentation procedure and three control tests were performed. The results from this experiment showed a force drop at 2.63 mm that corresponded to trend changes in both the inductance and SEI resistance. The combination of the force drop and change in ECM parameter value trends suggests that the internal physical structure in the damaged cell began to fail. These results are strongly correlated and show that fault detection is possible using the electrical response of Li-ion pouch cells in this study.

The experiments discussed throughout this study have major implications in non-invasive fault detection for battery management systems. Two of the three studies clearly show trend changes in ECM parameter values at the high to middle frequency range of the impedance spectrum. These studies show the possibility of detecting mechanical damage with EIS measurements and electrochemical process-based ECM modeling. These cells need to be further investigated to determine safety or remaining useful life of the cell. Continued research that incorporates electrochemical properties, various SOC, and loading scenarios can lead to accurate models for predicting the severity of mechanical damage. This research is only the start to establish promising techniques for assessing the integrity of LIB after sustaining mechanical damage and can lead to huge impacts in energy storage technology.

REFERENCES

- [1] A. Barai, G. H. Chouchelamane, Y. Guo, A. McGordon, and P. Jennings, “A study on the impact of lithium-ion cell relaxation on electrochemical impedance spectroscopy,” *J. Power Sources*, vol. 280, pp. 74–80, 2015.
- [2] Xiaopeng Tang, “A Fast Estimation Algorithm for Lithium-Ion Battery State of Health,” *J. Power Sources*, vol. 396, pp. 453–458, 2018.
- [3] Nicholas, Williard, “Lessons Learned from the 787 Dreamliner Issue on Lithium-Ion Battery Reliability,” *Energies*, vol. 6.9, pp. 4682–4695, 2013.
- [4] Xuning Feng, “Characterization of Penetration Induced Thermal Runaway Propagation Process Within A Large Format Lithium Ion Battery Module,” *J. Power Sources*, vol. 275, pp. 261–273, 2015.
- [5] B. Smith, “Chevrolet Volt Battery Incident Overview Report.” DOE NHTSA, 2012.
- [6] G. Kermani and Elham Sahraei, “Review: Characterization and modeling of the mechanical properties of lithium-ion batteries,” *Energies*, vol. 10, no. 11, 2017.
- [7] Elham Sahraei, “Dynamic impact response of lithium-ion batteries, constitutive properties and failure model,” *RSC Adv.*, vol. 00, pp. 1–10, 2019.
- [8] Elham Sahraei, John Campbell, and Tomasz Wierzbicki, “Modeling and Short Circuit Detection Of 18650 Li-Ion Cells Under Mechanical Abuse Conditions,” *J. Power Sources*, vol. 220, 2012.
- [9] Elham Sahraei, Rich Hill, and Tomasz Wierzbicki, “Calibration and Finite Element Simulation of Pouch Lithium-Ion Batteries for Mechanical Integrity,” *J. Power Sources*, vol. 201, pp. 307–321, 2012.
- [10] Lars Greve and Clemens Fehrenbach, “Mechanical testing and macro-mechanical finite element simulation of the deformation, fracture, and short circuit initiation of cylindrical Lithium ion battery cells,” *J. Power Sources*, vol. 214, pp. 377–385, 2012.
- [11] Yusuf Ali, Mohammed, Lai, Wei-Jen, and Jwo Pen, “Computational models for simulations of lithium-ion battery cells under constrained compression tests,” *J. Power Sources*, vol. 242, pp. 325–340, 2013.
- [12] Ilya Avedeev and Mehdi, Gilaki, “Structural Analysis and Experimental Characterization of Cylindrical Lithium-Ion Battery Cells Subject To Lateral Impact,” *J. Power Sources*, vol. 271, pp. 382–391, 2014.

- [13] Elham, Sahraei, Joseph Meier, and Tomasz Wierzbicki, "Characterizing and Modeling Mechanical Properties and Onset Of Short Circuit For Three Types Of Lithium-Ion Pouch Cells," *J. Power Sources*, vol. 247, pp. 503–516, 2014.
- [14] Mehdi, Gilaki and Ilya Avedeev, "Impact Modeling of Cylindrical Lithium-Ion Battery Cells: A Heterogeneous Approach," *J. Power Sources*, vol. 328, pp. 443–451, 2016.
- [15] Xu, Jun, Binghe Liu, and Dayong Hu, "State of Charge Dependent Mechanical Integrity Behavior Of 18650 Lithium-Ion Batteries," *Sci. Rep.*, vol. 6.1, 2016.
- [16] Dixon, Thomas, Elham Sahraei, and Tomasz Wierzbicki, "Dynamic Impact Tests on Lithium-Ion Cells," *Int. J. Impact Eng.*, vol. 108, pp. 205–216, 2017.
- [17] Dixon, Brandy, Amber Mason, and Elham Sahraei, "Effects of Electrolyte, Loading Rate and Location of Indentation on Mechanical Integrity of Li-Ion Pouch Cells," *J. Power Sources*, vol. 396, pp. 412–420, 2018.
- [18] Mehdi, Gilaki and Elham, Sahraei, "Effects of Temperature on Mechanical Response of Lithium Ion Batteries To External Abusive Loads," *SAE Tech. Pap. Ser.*, 2019.
- [19] Elham, Sahraei, "Modelling of Cracks Developed in Lithium-Ion Cells Under Mechanical Loading," *RSC Adv.*, vol. 5.98, pp. 80369–80380.
- [20] Elham, Sahraei, "Microscale Failure Mechanisms Leading to Internal Short Circuit In Li-Ion Batteries Under Complex Loading Scenarios," *J. Power Sources*, vol. 309, pp. 56–65, 2016.
- [21] L. Chen, Z. Lü, W. Lin, J. Li, and H. Pan, "A new state-of-health estimation method for lithium-ion batteries through the intrinsic relationship between ohmic internal resistance and capacity," *Measurement*, vol. 116, pp. 586–595, 2018.
- [22] D., Andre, "Characterization of High-Power Lithium-Ion Batteries By Electrochemical Impedance Spectroscopy. I. Experimental Investigation," *J. Power Sources*, vol. 196, no. 12, pp. 5334–5341, 2011.
- [23] E. Barsoukov and J. R. Macdonald, *Impedance Spectroscopy: Theory, Experiment, and Applications, 2nd ed.* Wiley-Interscience, 2005.
- [24] Ehsan Samadani, "Empirical Modeling of Lithium-Ion Batteries Based on Electrochemical Impedance Spectroscopy Tests," *Electrochimica Acta*, vol. 160, pp. 1639–177, 2015.
- [25] C. Pastor-Fernández, K. Uddin, G. H. Chouchelamane, W. D. Widanage, and J. Marco, "A comparison between Electrochemical Impedance Spectroscopy and

- incremental capacity-differential Voltage as Li-ion diagnostic techniques to Identify and quantify the effects of degradation modes within battery management systems,” *J. Power Sources*, vol. 360, pp. 301–318, 2017.
- [26] Ulrike, Krewer, “Review—Dynamic Models of Li-Ion Batteries for Diagnosis and Operation: A Review and Perspective,” *J. Electrochem. Soc.*, vol. 165.
- [27] Damoon Soubakhsh and Mehdi Gilaki, “Electrical Response of Mechanically Damaged Li-Ion Batteries.” .
- [28] S. H. Chung, T. Tancogne-Dejean, J. Zhu, H. Luo, and Wierzbicki, “Failure in lithium-ion batteries under transverse indentation loading,” *J. Power Sources*, vol. 389, pp. 148–158, 2018.
- [29] “GAMRY Instruments.’ [Online]. Available: <https://www.gamry.com/>.”
- [30] B. A. Boukamp, “A Linear Kronig-Kramers Transform Test for Immittance Data Validation,” *J. Electrochem. Soc.*, 1995.
- [31] S. Miller, “The Method of Least Squares.” .
- [32] C. Pastor-Fernandez, W. D. Widanage, and J. Marco, “Identification and Quantification of Ageing Mechanisms in Lithium-ion Batteries using the EIS technique,” *IEEE Transp. Electrification Conf. Expo*, 2016.
- [33] Bard and Faulkner, *Electrochemical Methods, Fundamentals and Applications*. Wiley, 2000.
- [34] S. Woo Han, “Transport and Kenetic Phenomena Linked to Power Performance of Lithium-Ion Batteries,” University of Michigan, 2014.
- [35] *Linear and Nonlinear Optimization*. SIAM, 2008.
- [36] Orazem and Tribollet, *Electrochemical Impedance Spectroscopy, 2nd ed.* John Wiley & Sons, Inc., 2017.
- [37] Lesel, “Mesoporous $\text{Li}_x\text{Mn}_2\text{O}_4$ Thin Film Cathodes for Lithium-Ion Pseudocapacitors.” NCBI, 2019.